THESIS FOR THE DEGREE OF DOCTOR OF PHILOSOPHY

Flow structures in solid-liquid suspensions in mixing and confined jets

MATTHIAS ENG

CHALMERS

Chemical Engineering
Department of Chemical and Biological Engineering
CHALMERS UNIVERSITY OF TECHNOLOGY
Gothenburg, Sweden, 2014

Flow structures in solid-liquid suspensions in mixing and confined jets

MATTHIAS ENG

ISBN 978-91-7597-089-9

Doktoravhandling vid Chalmers tekniska högskola
Serie Nr 2014:3770
ISSN 0346-718X

Department of Chemical and Biological Engineering
Chalmers University of Technology
SE-412 96 Göteborg, Sweden

Chalmers Reproservice
Göteborg, Sweden 2014

Flow structures in solid-liquid suspensions in mixing and confined jets

Matthias Eng
Department of Chemical and Biological Engineering
Chalmers University of Technology
SE-412 96 Göteborg, Sweden

Abstract

This thesis is an investigation of the influence of solid particles on different liquid flow systems. Large-scale periodic fluctuations such as macro instabilities (MI) and particle cloud dynamics in a mixing vessel and confined jets were studied experimentally and compared to numerical results from CFD simulations. The influence of particle size (0.5mm-2mm), volumetric concentration (0%vol-20%vol) and impeller speed (20Hz-37.5Hz) on turbulent structures and large-scale periodic phenomena were examined. Two-component Laser Doppler Velocimetry (LDV) measurements were conducted at different locations in a confined jet and in a mixing vessel. Video processing was used to observe the dynamic behaviours of a particle cloud and to track the cloud height. Spectral analyses were conducted using the Lomb algorithm to collect information about dominant periodicities in a continuous flow and particle cloud behaviour.

The flow conditions were numerically modelled with a Euler-Lagrange approach, treating the particles as a discrete phase and solving flow structures with an LES model. Numerical findings concerning MI phenomena, particle cloud spectra and local particle concentrations were compared to experimentally obtained data.

The results showed that all identified dominant frequencies were linear with impeller speed, resulting in a constant Strouhal number. The frequency of continuous-phase MI phenomena and of particle cloud dynamics was not influenced by the addition of solids. However, the amplitudes of the dominant frequencies in fluid MI phenomena, as well as in variations of particle cloud height, were reduced by increasing the concentration of solids. Spectra obtained with numerical simulations showed the same dominant frequency peaks as identified in the experiments. It was possible to track the local particle concentration inside a particle cloud and to detect the instantaneous cloud surface. The Root Mean Square (RMS) values in the confined jet increased at high particle loadings; the increase was particularly pronounced in the shear layer close to the nozzle. With increasing particle size, a greater effect on the RMS values could be observed. Large-scale instabilities in the jet could be identified in the spectra of the flow. The particles had a slightly stabilizing effect on the jet, and moved the instability downstream, while the frequency was unaffected.

Acknowledgments

I would like to thank everyone who has helped me in my work in the most recent years and made it possible for this thesis to be written.

First, I would like to thank Professor Anders Rasmuson for giving me the opportunity to do my PhD at Chalmers. And that, as my supervisor, he was always available, and spent time and energy giving me advice and putting me back on track.

For the technical help in building and repairing my equipment, I would like to thank Lars-Göran Johanneson and Jan Emnér. Gunnar Johannson is gratefully acknowledged for helping me with the LDV and for loaning me his equipment.

Special thanks to my close colleagues for sharing your work and your spare time. To Per who, as my roommate, shared many stories during the last years. And thanks to all my other colleagues and former colleagues who helped me and supported my project.

I want to thank my girlfriend Maria for supporting and encouraging me when I complained about the lack of progress in my work. And finally, special thanks to my lovely daughter Astrid, for cheering me up, distracting me and showing me what's important in life.

List of Publications

The compilation of this thesis is based on the following publications:

Paper I

Influence of solids on macro-instabilities in a stirred tank

Matthias Eng and Anders Rasmuson

Chemical Engineering Research and Design 90 (2012) 1052-1062

Paper II

Measurement of continuous phase velocities in a solid-liquid jet using LDV

Matthias Eng and Anders Rasmuson

Chemical Engineering Communications 201 (2014) 1497-1513

Paper III

Large eddy simulation of the influence of solids on macro instability frequency in a stirred tank

Matthias Eng and Anders Rasmuson

Chemical Engineering Journal 259 (2015) 900-910

Paper IV

Analysis of particle cloud height dynamics in a stirred tank

Matthias Eng, Rasmus Jonsson and Anders Rasmuson

Submitted (2014)

Contribution report:

Paper I

Main author. Planned the experimental outline, performed the experimental work and the analysis, interpreted the results.

Paper II

Main author. Planned the experimental outline, performed the experimental work and the analysis, interpreted the results.

Paper III

Main author. Planned the model outline, created the numerical model and the analysis, interpreted the results.

Paper IV

Main author. Active in planning the numerical model and experimental outline, performed parts of the experimental and numerical work, Active in analysis and interpretation of the results.

Contents

1

Introduction

1.1 General problem area

Multiphase fluids play a major role in most chemical processes. Whether this is the droplet flow in a spray or the mixing of two liquids or the fluidization of solid fuel particles, the interaction between phases will affect flow structures. While the flow of a single gaseous or a single liquid phase may be well understood for most flow situations, there is a lack of information on the description of multiphase conditions. More detailed investigations are needed to better understand turbulences, shear forces and the momentum transfer in a fluid under the influence of a secondary phase.

Numerical simulations in the field of multiphase systems improve continuously, but the tools are still limited to special cases. Models lack general validity especially for solid particles in the dispersed phase. Model assumptions and simplifications make it impossible to predict which influence inter-particle collisions, particle size or concentration have on the continuous phase. There are studies which model every particle separately in a flow, but due to computational demands, these studies are limited to small and idealized systems.

Experimental investigations of multiphase systems can deliver reliable data to observe and understand mechanisms in suspensions; at the same time they can give well needed information to improve and optimize numerical models. Laser-based optical measurement techniques are non-invasive, but limited to transparent flow systems. It is possible to investigate flow situations like bubble flow, droplet sprays and particle suspensions only to a certain extent using these techniques.

Stirred tanks are widely used in the chemical process industry. Mean flows using standard configurations are generally accepted to be well understood. Instantaneous flow, on the other hand, is extremely complex; it varies due to predictable mechanics like axis rotation and the passage of the blade of the impeller in a vessel, and unpredictable high frequency phenomena, turbulence and low frequency quasi-stationary phenomena. These low frequency phenomena are usually referred to as macro instabilities (MI) and affect the flow pattern in the vessel, which in turn affects large-scale mixing. Lifted particles in stirred vessels commonly form a dense particle cloud, which is separated from the clear liquid layer at the top. The height of the particle cloud, the local particle concentration and the residence time are important factors that influence mass and heat transfer in a suspension. Contrary to common assumptions, a particle cloud is far from stationary. Turbulent and periodic phenomena of a fluid affect particle behaviour in the cloud, and, as a consequence, the local particle distribution in a vessel will strongly vary in space and time.

Jet flows are one of the most common flow configurations. They occur directly as injection jet sprays or indirectly as part of more complex flow configurations such as fluidized beds, or the discharge of radial and axial mixing

impellers. Jets are characterized by a large velocity gradient between two fluids which builds up a shear layer. With increasing distance from the nozzle, jets can become unstable and large-scale vortices with a low frequency can then dominate the flow under this condition.

This thesis, and the papers presented herein, focus on the influence of solid particles on the flow properties of a liquid carrier phase. Solid particles in a liquid flow are a common but not very detailed investigated configuration in fluid dynamics and in the process industry.

1.2 Objectives

The objective of this thesis is to investigate in which ways flow structures in a mixing vessel and in a liquid jet are influenced by the presence of solid particles. The heat and mass transfer rates in processes involving solid particles are substantially dependent on the flow parameters of the suspension such as particle residence time, local particle concentration and relative particle velocity. It is, therefore, essential to understand particle-fluid interactions and the influence of flow properties in a suspension in order to predict process capabilities. Especially large-scale instabilities are of interest due to their ability to flush out particles from the bottom of a vessel and to vary the strength of the particle-carrying baffle jets.

Numerical models are an important tool in modern process planning and control. It is, therefore, of great importance to further develop multiphase models and particle-fluid interactions. To evaluate modelled data with results from identical experimental setups is an important step in identifying the strengths and weaknesses of current numerical models.

The height of a particle cloud is an important factor in solid-liquid suspensions, because it defines the degree to which particles are suspended in a fluid. The particle cloud surface is in opposite to common assumptions not stationary, but, rather, is characterized by dynamics that are not negligible. Understanding the connection between continuous-phase instabilities and particle-phase dynamics is vital to the development of numerical models and for obtaining reliable predictions of the flow properties of solid-liquid suspensions.
Having more knowledge about the turbulence structures, the velocity distribution and the mixing behaviour of solid particles in liquid flows is crucial to make these processes more efficient, to optimize quality and to improve the prevention of mechanical damage.

1.3 Outline of thesis

Solid-liquid suspensions with varying particle sizes and concentrations were experimentally observed and numerically modelled. Particles with different sizes were investigated to capture size dependencies of the solid-phase effect. Special interest is on turbulence variation and the influence of particles on large-scale instabilities. It is often mentioned that macro instability (MI) phenomena could cause an increase in the off-bottom suspension of solids and improve mixing due to their capability to break up the clear fluid layer which forms near the top of a stirred multiphase tank. Macro flow instabilities might also significantly influence the formation of the particle cloud in a suspension as well as the temporal and spatial variations of the local particle concentration.
Variations of the turbulence of the shear layer and of the large vortices would significantly influence the momentum transport in a jet. For this reason, large-scale jet instabilities play a major role in the distribution of solid particles from

the jet centre into the fluid bulk.

A two-component Laser Doppler Velocimetry (LDV) system was used to obtain velocity data on the continuous-phase flow in a mixing vessel and a confined jet. A numerical model was developed to compare flow simulation data with experiments. The formation and temporal variations of a particle cloud were investigated with experimental and numerical methods.

Post-processing of the data gave average velocities and RMS profiles. Frequency analyses of the flow and interpretation of the integral length scales were conducted to obtain further insight into the larger instabilities of the suspensions in a mixing vessel and in jets. The particle cloud height and local particle concentrations in a vessel were investigated with respect to their temporal and spatial variations. Dominant periodic behaviours could be identified and compared to macro instabilities in the continuous-phase flow.

2

Background

2.1 Fluid dynamics of particles

Depending on particle concentration, particle momentum and the flow structures of the carrier phase, different phenomena can dominate the description of particle flow (Crowe et al. [1]). A flowing fluid applies forces on a particle in a suspension. Due to these forces, which make the particle flow in a fluid, the particle will change direction and velocity. The extent to which flow can influence particle movement is dependent on the ratio between particle inertia and drag. A particle with a low mass will more easily follow a fluid flow than a high-density particle.

$$Stokes = \frac{\tau_p}{\tau_i} \tag{2.1}$$

$$\tau_p = \frac{\rho_p d^2}{18\mu_l} \tag{2.2}$$

The particle Stokes number is an important measure of fluid-particle interaction. The Stokes number describes the ratio between the particle relaxation time and a characteristic time scale of the flow (Equ.2.1). The particle relax-

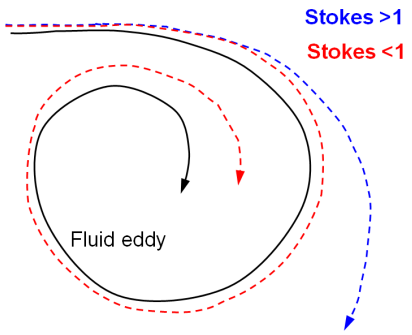

Figure 2.1: Trajectories of particles with different Stokes number

ation time (Eq.2.2) is a measure of the ability of a particle to be influenced by a flow, which, as mentioned, can be described as the relation between particle inertia and drag. The characteristic time scale of a flow relates to a certain fluctuation or change in the direction of the flow. If the Stokes number of a particle is significantly larger than one, the particle trajectory will barely be influenced by a flow structure with this time scale (Fig.2.1). For a Stokes number considerably smaller than one, it can be assumed that the particle will follow the fluid flow to a very large extent. If the Stokes number is equal to one, then the fluid flow and the particle will have the same time scale and will influence each other.

A fluid will be influenced as well by the presence of particles. A fluid and particles are in a permanent state of exchange of momentum. Due to their inertia, particles can slow down a decrease in fluid velocity, but will also take kinetic energy from the fluid when accelerating. This interaction is not completely clear when particles are confronted with fluid turbulence. Particles can cause turbulence and they can inhibit fluid turbulence, depending on the size of a certain eddy and the particles. A particle flowing in a fluid with certain slip velocities will cause turbulence due to vortex shedding (Fig. 2.2). Small vortices separate at the surface and form a wake after the particle. Turbulence

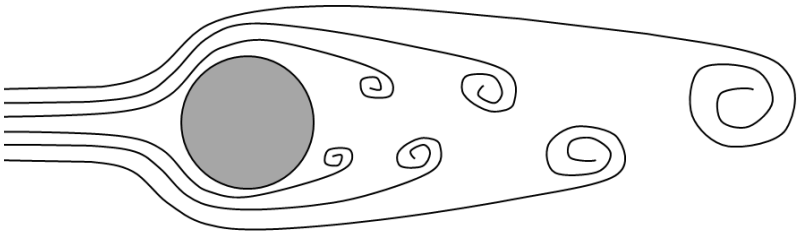

Figure 2.2: Augmentation of turbulence due to particle vortex shedding

is produced by extracting kinetic energy from the fluid, and this could be called an augmentation of turbulence due to particles. However, particles can also attenuate turbulence. If a particle is confronted with an eddy which it cannot follow, it will flow through the eddy and break it. The resulting smaller eddies will dissipate faster, and in this way turbulent energy will be reduced by the particle.

Gore and Crowe [2] have defined a ratio d_p/Λ between particle diameter and the size of the energy-carrying vortex (integral length scale). If this ratio becomes larger than 0.1, the particles cause an augmentation of the turbulence, while for values lower than 0.1 the particles attenuate the turbulence in the carrier phase. As discussed in Paper II, the value for the integral length scale varies significantly between different locations in a flow. In contrast to the Stokes number, neither the density nor the viscosity is considered in this value. The ratio d_p/Λ gives information about the size scales at which turbulent production outweighs enhanced turbulent dissipation.

With greater particle concentration, particle-particle interaction becomes more relevant. When two particles collide with each other, they not only exchange momentum, but change their trajectory significantly. Particles obtain a strong component through collisions, and this is directed orthogonal to the fluid flow. Depending on particle inertia, a certain distance is necessary before the par-

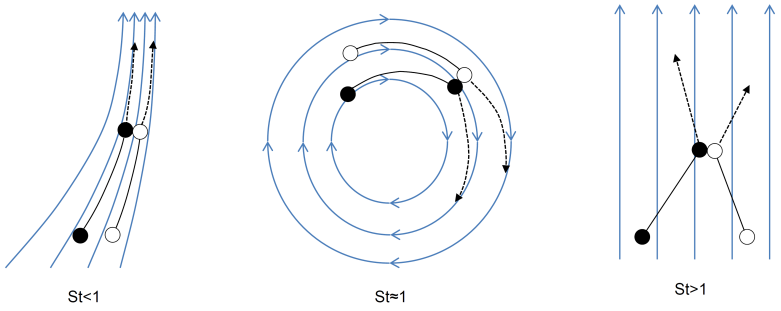

Figure 2.3: Inter particle collision behaviour with different Stokes number

ticles adapt to the fluid flow direction and velocity again. During this time, the particles transfer their momentum to the continuous phase. In this way, particles enhance the exchange of momentum between different regions of fluid flow and generate much greater particle dispersion.

Gravitation is also an important factor for larger particles; solid particles will always tend to fall to the bottom of the flow configuration and the energy to lift them or keep them suspended must come from the kinetic energy of the flow. In the present study, only solid glass particles are discussed, they can always be assumed to be spherical and of identical size. For this reason, agglomeration, breakup and variation of shape can be neglected.

$$Stokes_c = \frac{\tau_p}{\tau_c} \tag{2.3}$$

The collision Stokes number (Eq.2.3) is the relation between particle relaxation time and the time scale of inter-particle collisions (τ_c). Crowe et al. [1] use the collision Stokes number to quantify whether a particle flow is dilute or dense. Particle-particle interaction in dilute flows is of minor significance, because the distance between the particles is large and collisions are rare. For all investigated flow conditions in this thesis, in the mixing vessel as well as in the jet,

a collision Stokes number larger than one was identified. Consequently, all the investigated cases can be described as dense two-phase flows. In dense flows, particle-particle interaction is not negligible. Collisions occur often and play a major role in the transfer of momentum.

The collision behaviour of particles in a viscous fluid varies with different particle Stokes numbers (Choi et al. [3]). Particles with a small Stokes number flow parallel to the fluid streamlines with a similar velocity. Collisions between these particles happen mainly due to flow fluctuations and accelerations, while the colliding particles have similar trajectories. The particles have only a minor change in trajectories after a collision, and shortly after will follow the fluid streamlines again (Figure 2.3). Particles with large Stokes numbers only follow the fluid flow to a certain extent; their trajectories can differ a lot from fluid streamlines. Due to large differences in velocity and direction, collisions between these particles can be very strong and can cause significant changes in the trajectories of particles. A particle is able to move a far distance even in directions crossing fluid streamlines, because particle inertia is dominant. In this way, particles can travel into different flow regions as a result of collisions and transfer momentum to the fluid or to other particles.

2.2 Flow structures in mixing vessels

2.2.1 General

Mixing is one of the most common processes in chemical engineering. There are numerous different configurations of mixing equipment for specialized purposes. Two main configurations are axially agitated and radial agitated mixers. In a radial agitated mixer, the impeller is of the Rushton-type with varying numbers

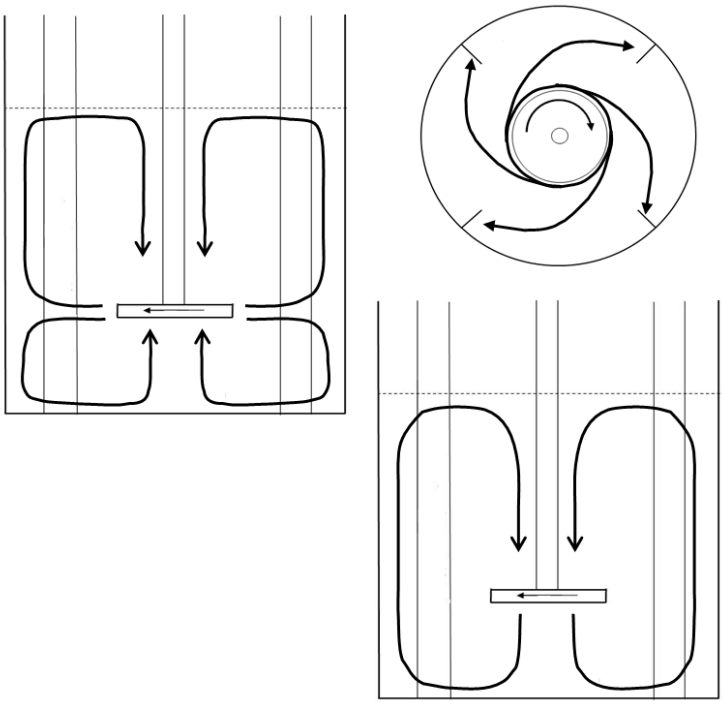

Figure 2.4: General flow in different mixing vessels

of blades. The fluid is discharged from the impeller in the radial direction and when it impinges on the walls of the mixing vessel it splits in upwards and downwards flows. Rushton-type mixing vessels are characterized by double flow loops; one upper and one lower flow loop (fig. 2.4). Axially agitated mixers have a pitched-blade turbine (PBT) impeller, which discharges the fluid in the axial direction. If the impeller jet is directed downwards, a strong jet hits the bottom and splits to create a strong upwards-directed jet at the vessel walls (Hasal et al. [4]). Axially agitated mixers are characterized by this strong upwards jet and one flow loop which carries the fluid from the bottom of a vessel to the surface and back into the vessel centre (fig.2.4).

Close to the impeller, the flow is dominated by strong turbulence. Especially Rushton impellers produce very large shear forces at the blades, which in gas-liquid suspensions is used for bubble breakup and dispersion. Impellers with an axial discharge produce less shear, especially when the blades are aerofoil

shaped. All impeller styles induce a strong rotational component to the flow, which can only be broken by static baffles on the vessel walls. Baffles prevent the flow from just rotating in the vessel, but they also cause strong shear forces and turbulence.

In the study in Paper II, a 45Ð PBT was used to stir the suspension, because an axial discharge jet has great advantages when lifting heavy particles off the bottom of a vessel. In this setup, solid particles are carried upwards and dispersed by the strong jet-like flow close to the baffles. The energy to lift heavy particles off the bottom and to keep them dispersed must be taken from the kinetic energy of the flow. With greater particle concentration, the flow velocities decrease. At the same time, the fluid is no longer able to lift the particles to the surface of the vessel and a cloud of particles is formed which does not fill the upper region of the vessel. This particle cloud phenomenon has been the object of numerous investigations, e.g., Bittorf and Kresta [5] and Bujalski et al. [6]. An often used criterion to estimate the cloud height for a certain solids loading is given by Zwietering [7].

2.2.2 Macro instabilities

Macro instability (MI) phenomena are large-scale flow instabilities that occur in mixing processes. The general flow field as described in 2.2.1 in a mixing tank features not only strong turbulence but also large periodic changes in flow direction and velocity. In contrast to high frequency turbulence and the high rotational speed of the impeller, an MI phenomenon is characterized by a low frequency. MI phenomena can be recognized throughout a mixing vessel, but their dominance varies at different vessel locations (Kilander et al. [8]). The periodic change in the mixing flow plays a major role in the mixing process in

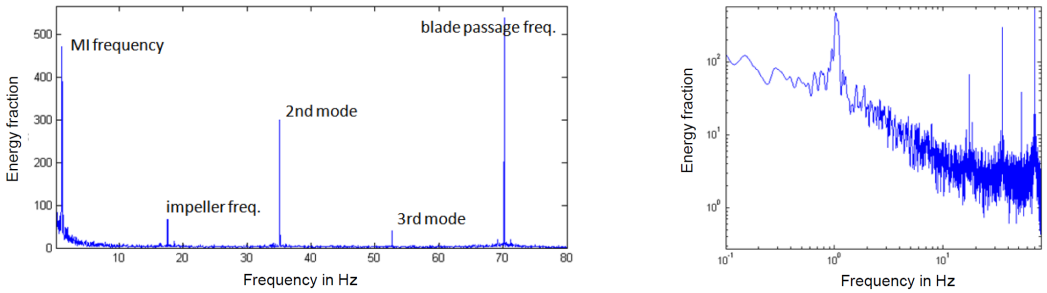

Figure 2.5: Lomb spectrogram with MI frequency and impeller frequencies in linear- and log-scaling

a vessel. As an addition to the general flow loop, an MI phenomenon enhances the interchange of fluid packages. Yianneskis et al. [9] have described the MI phenomenon as a precession vortex around the impeller shaft in a mixing vessel. The frequency of MI phenomena is linearly related to the rotational speed of the impeller in a vessel; therefore a Strouhal number (S) or a non-dimensional frequency is often used to describe MI phenomena.

Results obtained in the present study have been used for the following explanation of an MI phenomenon. With a frequency analysis using the Lomb algorithm 3.3.1, the energy content of each frequency in a flow can be identified. Figure 3.6 shows a typical spectrogram with a strong peak, which describes the macro instability phenomenon in the flow. The non-dimensional MI frequency $S_{MI} = f_{MI}/f_{impeller}$ was identified as 0.06. Figure 2.5 shows a spectrogram of a typical flow situation in relative proximity to the impeller in a mixing vessel. The impeller frequency can be identified as 17.5Hz and the blade passage frequency for a four-bladed PBT impeller as 70Hz. The macro instability had a low frequency of only 1.06Hz in this case. Figure 2.5 also shows the logarithmic-scaled version of the spectrogram, which is commonly used when analysing turbulence, but has disadvantages in a low frequency analysis.

Chapple and Kresta [10] have concluded that an MI phenomenon occurs due to interaction between the impeller in a vessel, the baffles and vessel geometry. Galletti et al. [11] have found that the linear dependence between the frequency of the MI phenomena and the rotational speed of the stirrer exhibits different proportionality constants for low, intermediate and high Reynolds number flows. They have also found, using both a PBT and a Rushton turbine, that the off-bottom clearance of the impeller has no significant effect on the frequency of the MI phenomena. They did, however, find that the frequency changed when the ratio between the impeller diameter and the tank diameter changed.

$$\tau_i = \frac{1}{f_{MI}} \tag{2.4}$$

MI phenomena are of interest especially for the dispersion of solid particles. Solid particles cannot follow fast turbulent fluctuations, but a low frequency instability is able to transport heavier solids. There are very few investigations into how MI phenomena are influenced by the presence of solids. Jahoda et al. [12], for instance, have found a significant decrease in the frequency of MI phenomena at a solids loading above 10%(w/w). Paglianti et al. [13] have investigated a concentration of 40%(w/w) and found a lower frequency of MI phenomena in the suspension than in the single-phase flow. Bittorf and Kresta [5] have observed a disappearance of MI phenomena at high solid concentrations, which coincided with the appearance of a clearly defined cloud height. The present study tries to relate the interaction between particles and MI phenomena to the particle Stokes number (eq.2.1). As a characteristic time scale of the flow τ_i , the reciprocal of the frequency of MI phenomena was used. With the definition from Equation 2.4 the particle response time was related

to the time scale of the MI phenomena. For the particles used in Paper II, this leads to values between 0.28 and 1.1, as shown in Table 3.1.

2.3 Particle cloud height

The agitation in a mixing vessel causes the heavy solid phase to be lifted off the bottom of the vessel, in this way a solid-liquid suspension is formed. The lifted particles often form a cloud which is clearly separated from the clear liquid layer at the vessel top. The well-known Zwietering (Zwietering [7]) criterion gives information about the required impeller speed and energy to achieve just-lift-off conditions, meaning no stagnant particles on the bottom of the vessel. The Zwietering criterion is commonly used in all kinds of solid liquid suspensions to estimate impeller speed and power demands for mixing. This estimate, however, does not consider any temporal or spatial variations of the particle cloud and lacks any description of cloud formation. It is known that the mixing flow in agitated vessels is very complex, and so is the formation of a particle cloud.

Sardeshpande et al. [14] have observed significant differences in the height of the particle cloud at different locations in a vessel and have described temporal variations. The study by Bittorf and Kresta [5] focuses on the prediction of a time-averaged cloud height and discusses the role baffle jets play in cloud formation, i.e. baffle jets carry solid particles into the upper region of a mixing vessel. Studies of single-phase conditions describe baffle jets as dominated by macro-scale instabilities (Bruha et al. [15] and Bruha et al. [16]). Consequently, this would cause strong temporal variations of particle cloud height and cloud location in a solid-liquid suspension. Figure 2.6 shows a schematic view of the

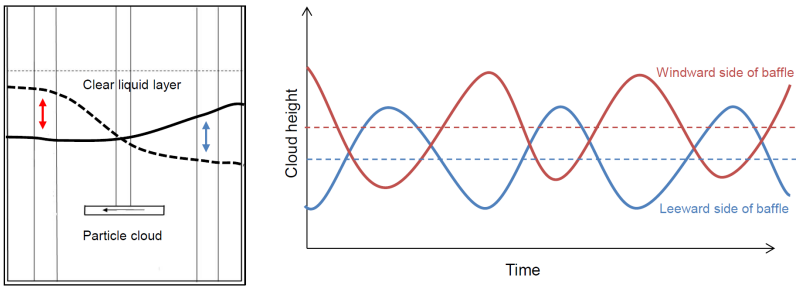

Figure 2.6: Schematic view on the spatial and temporal cloud height variations

particle cloud height at two different locations in a vessel and the temporal variations at these locations.

The formation of a particle cloud is not only dependent on impeller speed, but also particle size, density and concentration have a significant impact on the behaviour of a suspension. Systems with low concentrations and comparably light particles behave like dilute suspensions. With increasing particle concentration, inter-particle collisions become more significant. The particles get their momentum from the agitated continuous phase, but through collisions they exchange momentum with each other so strongly that they behave like a common unit and form a cloud.

2.4 Flow structures of a particle suspension jet

Jet flow is a special case of shear flow that is characterized by a very strong velocity gradient between two fluids. The most common case is an injection jet where fluid is injected at a high velocity into a stagnant fluid bulk. However, jets also occur as part of more complex flow systems, such as jet mixers, the discharge jet from a mixing impeller, the flow over a step or in flows with a high velocity difference.

Due to viscous shear, momentum is transferred between a high velocity jet and

the surrounding fluid. As a result, the centreline velocity of a jet decreases with increasing distance from the jet origin, while the width of the jet expands. This flow has all the properties of a pipe flow at the exact location of the nozzle exit. Directly after the nozzle, the jet interacts with the surrounding fluid and a shear layer develops. While the core of the jet still has the properties of the pipe flow, the shear layer between the jet and the surrounding fluid is dominated by high turbulence.

Turbulence is produced in the region of high shear by extracting kinetic energy from the main flow. High turbulence intensity indicates a large transfer of momentum between fluid layers. A three-dimensional free jet typically expands at an angle of 10° while the shear layer grows and swallows the jet core. At this point, the jet becomes substantially exchanged with the surrounding fluid and has high turbulent kinetic energy; although turbulent production and dissipation are in equilibrium. At a farther distance from the nozzle, the dissipation of turbulent energy takes over and the main flow decreases further until any gradient between the jet and the surrounding fluid is equalized. Single-phase jet flows have been included in many studies, some of the most famous and detailed are, e.g., by Townsend [17], Hinze [18], Wygnanski and Fiedler [19] and Gore and Crowe [2].

Influenced by external factors, a jet will become unstable Batchelor and Gill [20]. After a certain distance from the nozzle, the jet will begin to fluctuate around the centreline and the flow will become dominated by large-scale vortices. The large-scale vortices of a jet instability significantly enhance the exchange of momentum and mass, and the surrounding fluid is, thus, entrained into the main flow. This instability is of importance, particularly when considering the mixing behaviour of a solid-liquid suspension. Large-scale vortices are

slow and particles in a suspension are able to follow them, which significantly increases the dispersion of solids.
Particles of different sizes affect a flow differently, and the relations of the flow to length and time scales are important. Particles influence, as described in 2.1, the turbulent structures of a fluid flow. By breaking bigger vortices into smaller eddies, turbulent kinetic energy is dissipated faster, but particles can also add turbulence to a flow. These influences on the energy cascade of turbulence affect the transport of momentum, mass and heat. Many studies have investigated the influence particles have on a jet in gas-solid suspensions, but only very few have investigated solid-liquid suspensions.

Most studies have concluded that particles in a gas flow enhance the experienced viscosity, and that the axial flow profiles are flatter and the decay of the centreline velocity decreases, e.g. Fan et al. [21] and Sheen et al. [22]. Gore and Crowe [2] have suggested that an augmentation of turbulence occurs due to particles when the ratio between the particle diameter and the integral length scale (equ.3.8) of a flow is larger than 0.1; in contrast, particles cause an attenuation of turbulence at a value smaller than 0.1. While the integral length scale refers to the size of the energy-carrying eddies, the Stokes number also includes the viscosity and the density difference between particle and fluid. Identifying the characteristic time scale of the flow in a jet is not possible without measurements or detailed simulations. Therefore, Hardalupas et al. [23] have defined a semi-empirical formulation to determine the particle Stokes number at different flow conditions as a function of the distance from the nozzle (eq. 5.1). They have described an increase in Stokes number with increasing nozzle distance, which is connected to the decrease in flow speed and the increase in the size of eddies.

A change in Stokes number means that particle influence changes with distance from the nozzle. Parthasarathy [24] have investigated how particles influence the instability of a gas-solid jet. They found a decreased instability frequency and a flow stabilizing effect due to particles.

3

Experimental methods

3.1 Equipments

3.1.1 Paper I - Mixing vessel

The study of a particle-laden flow in a mixing vessel was conducted in a model made entirely of glass. The flat-bottomed cylindrical tank had a diameter of T=150mm and was filled up to a height equal to its diameter T=H. The suspension was axially agitated by a 4-bladed 45° PBT with a diameter of D=T/3 and no hub. The tank was equipped with 4 baffles with a width of B=T/15=10mm. The impeller rod, the blades and the baffles were made of steel. The ground clearance of the impeller was kept constant at C=T/3. The convex surface of a cylindrical vessel is problematic when conducting measurements with an optical technique such as LDV. To prevent the laser beams from approaching from an angle that is too steep, the tank was placed in a square glass tank filled with water. This ensured an approach angle of 90° on the glass surface and only a small refraction to be overcome when the beam entered the mixing vessel.

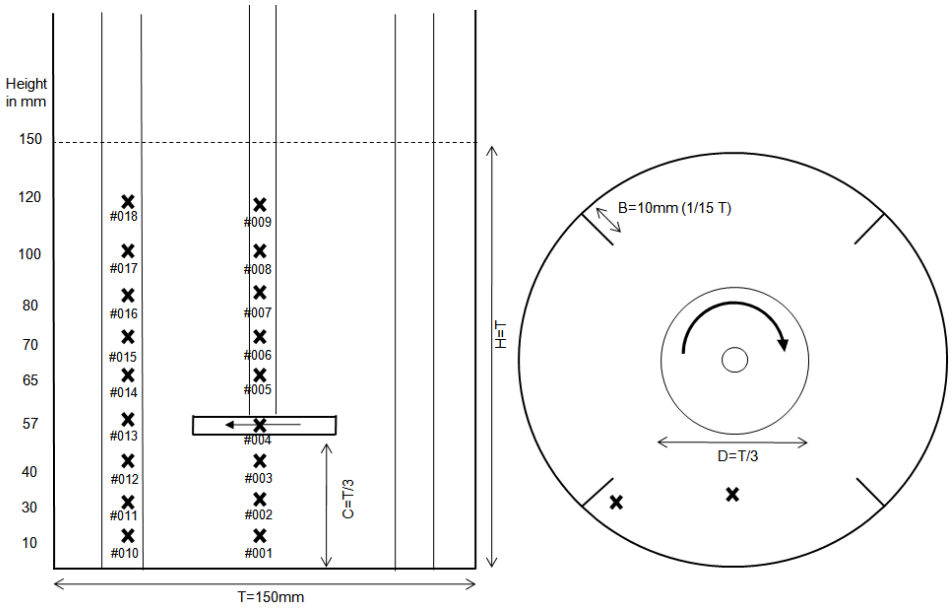

Figure 3.1: Measurement configuration of the mixing vessel

Measurements at 18 different locations, separated into two vertical rows at 9 locations, were conducted in this study. The measurements #001 - #009 were located in the vessel bulk at half the radius of the vessel centreline. The measurements #010 - #018 were located close to the vessel wall on the windward side of the baffle, where the strongest influence of MI phenomena was expected. Figure 3.1 shows the setup and the measurement locations in the mixing vessel.

3.1.2 Paper II - Confined jet

Studying the flow properties of gaseous jets is usually done in radially symmetric jets injected into free space. Dealing with a liquid flow medium is by far more difficult. The liquid medium must be pumped in a loop, all components must withstand the water pressure, and the tank dimensions are somewhat limited in size. It is, therefore, not feasible to study a radially symmetric jet, but rather a jet confined between two narrow walls in one direction while free to expand in the lateral and axial directions. When adding particles to a liquid

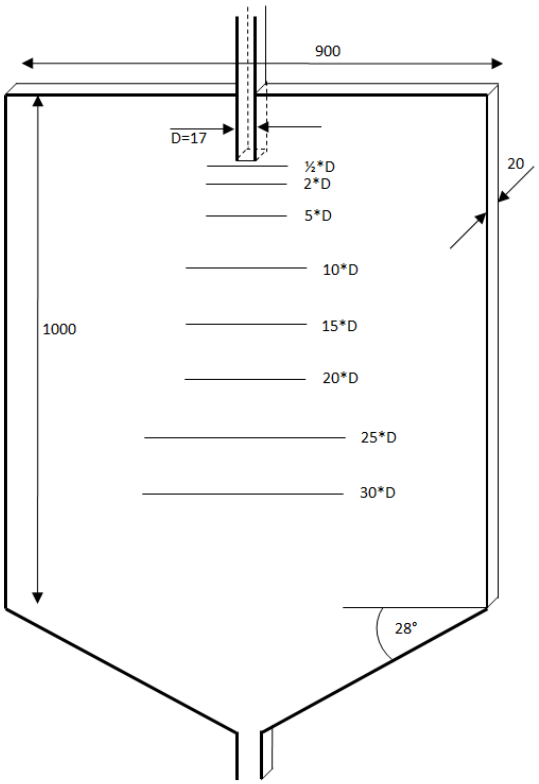

Figure 3.2: Measurement configuration of the confined jet

flow loop the possibility of particle accumulation in the equipment must be considered. Buffer tanks, horizontal pipe sections and flat bottomed tanks are not applicable.

For the confined jet study in Paper II, a special tank was constructed to satisfy all the demands of the optical measurement technique and the suspension used. The equipment was comparable in all geometrical aspects to the equipment used by Virdung and Rasmuson [25]. A large glass tank with the measurements 1000mm*900mm comprised the centre part of the setup; the suspension was injected through a square nozzle (17mm) 100mm under the liquid surface (fig. 3.2). With a depth of only 20mm, the tank was only 1.5mm wider than the nozzle on each side. This way, the jet was constrained in its expansion and the lateral and axial flow components dominated. Although the average

flow in the constrained direction might be zero, flow turbulences were three-dimensional and fluctuations in the constraint directions were not completely negligible, but were expected to be minor.

The tank was completely filled with water, equipped with a lid and ventilated through a small opening. The tank was entirely made of glass to maintain optical accessibility. To prevent particles from accumulating in the tank, the bottom was conically shaped with an angle of 28°, that led directly into the pump. All pipe sections were designed to avoid horizontal parts. The suspension was continuously pumped with an excenter screw pump in a closed-flow loop without any additional buffer tanks. This can cause unwanted flow disturbances originating from pump fluctuations, but it was necessary to maintain a constant particle concentration in the inlet nozzle. Certain frequencies caused by pump rotation and vibrations were registered in the spectrograms close to the nozzle, but disappeared at farther axial distances.

3.1.3 Paper IV - Particle cloud

Particle cloud behaviour was investigated in the same axially agitated mixing vessel as in Paper I (Fig. 3.1). The experimental method was based on high definition videos which were taken of the mixing vessel to observe particle behaviour. In order to be able to investigate the particle cloud in a specific region, a strong light source was placed at the side of the vessel and a visor was positioned in a way that only the particles closest to the camera were illuminated (Fig. 3.3). Each case was filmed for 30s with 25 full frames per second at a resolution of 1080x1920 (1080p25) resulting in 750 frames.

Further post-processing of the video data was done in Matlab, where a frame grabber extracted each frame to create picture files. Using the fixed frame rate

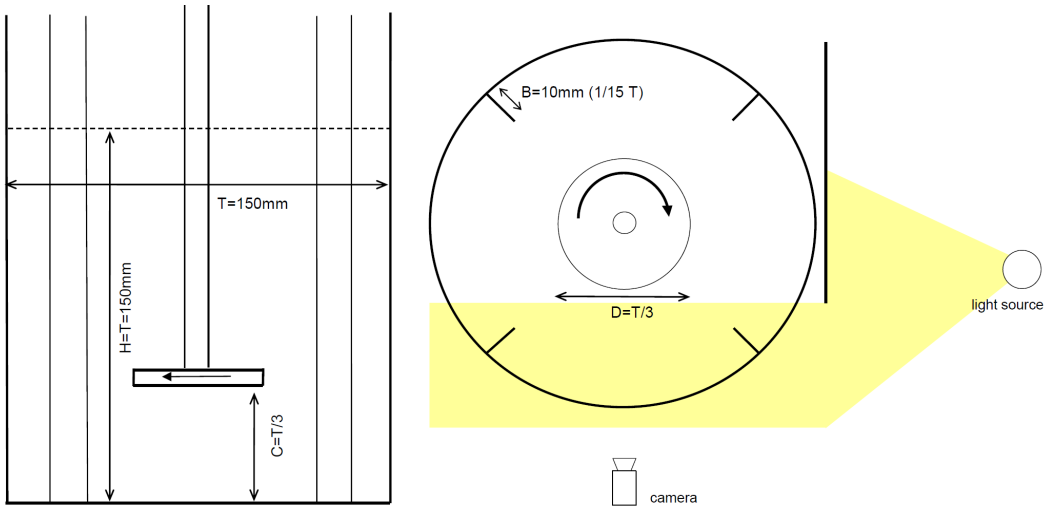

Figure 3.3: experimental setup for particle cloud study

of the video, the time steps between each picture were identified. The contrast of each frame was increased to improve the separation between bright particles and dark background. Figure 3.8 shows a typical frame after post processing.

3.2 Laser Doppler Velocimetry - LDV

Most measurements presented in this thesis were obtained by means of Laser Doppler Velocimetry (LDV). LDV is a non-invasive optical measurement technique used to determine velocities Durst et al. [26]. The LDV system used in the studies was a commercial system from Dantec Measurement Technology; the FiberFlow dual beam system (Series 60X). Figure 3.4 shows a schematic view of the LDV setup. The light source was a Spectra-Physics water-cooled 6W Ar-ion laser model Stabilite2017. In the transmitter unit, the laser light was split into two beams and separated into the three most dominant wavelengths. In the setup for the mixing vessel (Paper I), only one wavelength (514.5nm) was used, while two wavelengths (514.5nm and 488nm) were used

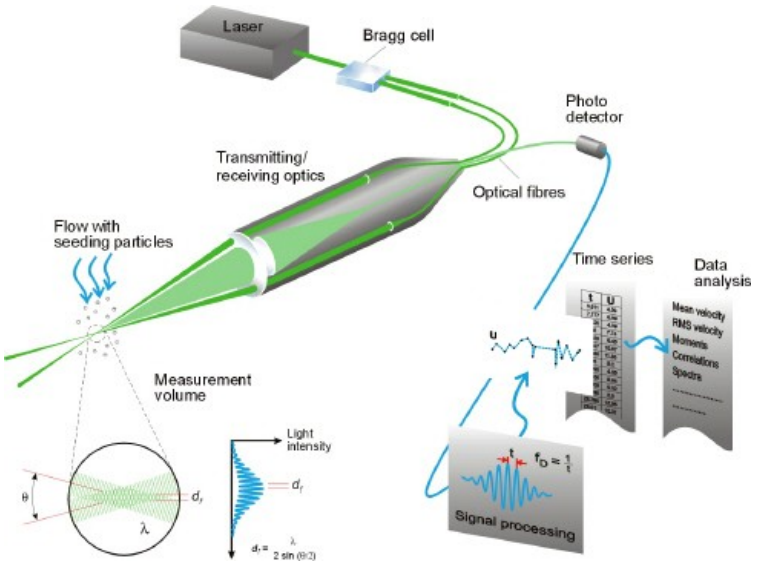

Figure 3.4: Principle of Laser Doppler velocimetry - Dantec Dynamics

in the study of the confined jet.

Fibre optics transported each beam to the main LDV probe, from there they were guided into the measurement section. Two beams of the same wavelength (the same colour of light) crossed at 310mm from the lens at the focal point. All beams were focused with an expansion factor of 1.98, so that the intersection volume, which forms the measurement volume, was kept as small as possible. A small measurement volume guaranteed a large spatial resolution and yielded, in this case, a volume length of 702 microns and a diameter of 76 microns. The intersecting beams formed an interference pattern of dark and bright zones, so called fringes. LDV cannot measure velocities of a perfectly clear fluid; consequently small tracer particles are needed. Dantec 9080A7001 silver-coated hollow glass spheres with a diameter of 10 microns and a density of density of $1.3 kg/dm^3$ were used in this study. They were small enough so their inertia could be neglected and their velocity was assumed to be equal to the liquid flow. When a tracer particle that is sufficiently small flows through a measurement volume, it reflects the dark and bright zones.

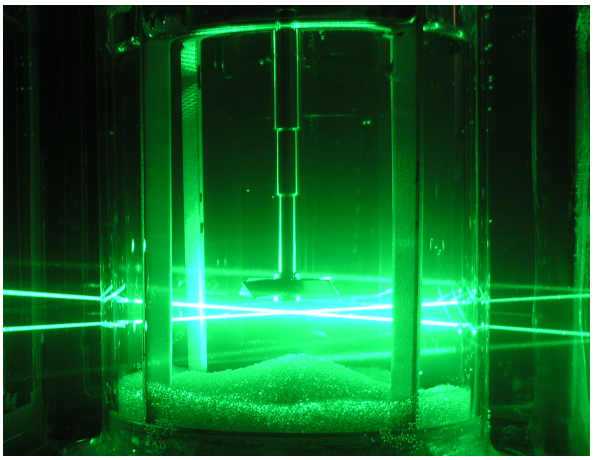

Figure 3.5: Laser based velocity measurements in solid-liquid suspension

Depending on the velocity of the tracer, a reflection function, a so called burst, can be received. The probe also functions as a receiving unit, which means that the LDV was operated as a backscatter system. The light received by the probe was split into the different wavelength components again, and the light of each wavelength was sent to a photo multiplier where the light signal was converted into an electric signal. The electric signal was processed in a Burst Spectrum Analyser (BSA). The BSA separated valid tracer bursts from the background noise, and each burst signal was stored as a velocity value.

Only the velocity perpendicular to the fringes can be determined from the interference pattern of two laser beams, which is related to only one flow component. If a second velocity component is desired, an additional pair of beams must be used to create an interference pattern perpendicular to the first one, but at the same intersection point. To be able to separate reflected light from both components, light with different wavelengths was used for each pair of beams. In Paper II, for example, light with a wavelength of 514.5nm was used to measure the axial velocities in the jet and a wavelength of 488nm was used to measure the lateral velocities. To be able to measure flow with zero velocity and to alternate between positive and negative flow directions, the interference

patters were constantly moved at a speed much higher than the expected flow. The movement of the interference pattern was achieved by shifting one beam of each pair at a frequency of 40MHz.

The data, including arrival time, transit time and the velocity of each tracer detected, were sent from the BSA to the windows-based BSA flow software, version 2.12.00.15. The software allowed for the monitoring of ongoing measurements and controlling the measurement setup including the measurement locations. To maintain a high data rate, the data-obtaining settings of the BSA must be adjusted to the predominant measurement conditions. The high voltage going to the photo multiplier can be adjusted to increase the electric signal, but this will also increase existing noise, while the signal gain amplifies signal peaks. A signal gain of 44db and a high voltage of 1,216 V were chosen for measurements in the mixing vessel, while a signal gain of 32db and a high voltage of 1,567 V were chosen for the flow measurements in the confined jet. The velocities of large particles in solid-liquid suspensions will be different from fluid velocity. Therefore, one must be careful to observe that the LDV correctly distinguishes the signals received by the tracers and reflections from the particles. In the suspensions investigated, the particles were dimensions larger than the tracers and also larger than the diameter of the measurement volume. In these suspensions, the reflection from a particle looked significantly different from the one from a tracer. While a tracer reflects the interference pattern, larger particles solely reflect the average light intensity. The BSA is able to separate these signals and exclusively allow valid bursts from the tracer by using the oversize rejection setting. More detailed information can be found in Durst et al. [26].

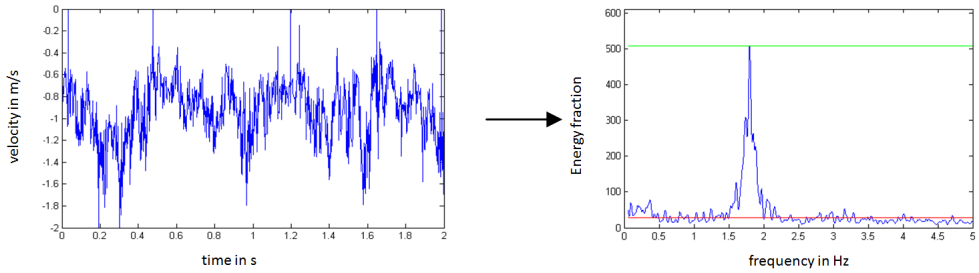

Figure 3.6: Analysis of typical velocity data into a frequency spectrogram

3.3 Data processing

3.3.1 Lomb algorithm

The LDV technique measures instantaneous velocity values with a very high data rate. In instationary flow situations, this gives a temporal distribution of the velocity at each location. Besides the average velocity, the measured data also contain information about turbulent kinetic energy, vortex length scales and periodic flow phenomena.

There are two common ways for analysing frequency spectra; either using the Fourier transform or using the Lomb algorithm Lomb [27]. LDV detects a velocity value the moment a tracer flows through the measurement volume. This occurs randomly distributed around the average data rate. LDV data, in contrast to hotwire or PIV measurements, are not obtained with a fixed temporal resolution, but instead have an unequal temporal distance between measured values. The Fourier algorithm requires equally spaced data, however, which would make it necessary to resample the LDV data by deleting values and filling gaps with estimated ones. The Lomb algorithm is able to handle non-equally spaced data, can handle the raw data from the LDV and was, therefore, used throughout this study. For the input data h, the Lomb algorithm becomes

Press et al. [28],

$$\langle h \rangle = \frac{1}{N} \sum_{i}^{N} h_i \tag{3.1}$$

$$\sigma^2 = \frac{1}{N-1} \sum_{1}^{N} \left(h_i - \langle h \rangle \right)^2 \tag{3.2}$$

$$\omega = 2\pi f \tag{3.3}$$

$$\tan\left(2\omega\tau\right) = \frac{\sum_j \sin 2\omega t_j}{\sum_j \cos 2\omega t_j} \tag{3.4}$$

$$P_N\left(\omega\right) = \frac{1}{2\sigma^2} \left\{ \frac{\left[\sum_j \left(h_j - \langle h \rangle \right) \cos\omega\left(t_j - \tau\right)\right]^2}{\left[\sum_j \cos^2\omega\left(t_j - \tau\right)\right]} + \frac{\left[\sum_j \left(h_j - \langle h \rangle \right) \sin\omega\left(t_j - \tau\right)\right]}{\left[\sum_j \sin^2\omega\left(t_j - \tau\right)\right]} \right\} \tag{3.5}$$

The probability of $P_N\left(\omega\right)$ between i and $i + di$ is $e^{-i}di$. Consequently, if we look at M independent frequencies the probability that none of them will give a larger value (i) is $\left(1 - e^{-i}\right)^M$. One disadvantage of the Lomb algorithm is that it is computationally heavier than the FFT, and the amount of operations scale with the number of data points, N, as N^2. The in-house code was based on the C code given by Press et al. [28] and written in Matlab R2011 in order to calculate the Lomb spectrogram.

Figure 3.6 shows a typical velocity plot as obtained by the LDV, and the corresponding spectrogram after Lomb analysis. A certain periodically large fluctuation can be identified as early as in the velocity plot. In the spectrogram this appears as a clear peak with a low frequency. The energy fraction inherent to each frequency of the flow was analysed with the Lomb algorithm and illustrated in a spectrogram. Dominant frequencies in a flow will contain a large fraction of the energy, and, therefore, will cause high amplitude in the spectro-

gram. Thus, periodic flow phenomena can be identified and their strength can be evaluated.

3.3.2 Signal to noise ratio

The amplitude in the Lomb spectrogram gives a measure of the energy fraction of each frequency in relation to flow energy. With a spectrogram, one can identify dominant flow frequencies, periodic phenomena and the energy dissipation of turbulences with high frequencies. The absolute amplitude in the spectrogram is not suitable for qualitative evaluations of the strength of a periodic phenomenon when comparing different measurement conditions.
A measurement series was conducted in which the physical flow conditions and measurement location were maintained while the measurement parameters, such as laser power or signal gain, were varied in order to manipulate the data rate of the measurements. The investigated instability could be identified at identical frequencies under all measurement conditions, but the maximum amplitude did show a notable dependence on the data rate. To be able to compare the strength of instabilities in different suspensions, an analysis method is needed which is independent of the measurement data rate. This is especially needed when investigating suspensions with different concentrations of solids, because denser suspensions create less perfect conditions for LDV, consequently causing a lower data rate.

A solution to this problem is to use the ratio between the maximum peak amplitude and the average background noise of each measurement. It was observed that when the maximum amplitude of a peak decreased due to a low data rate, so did the amplitude of the background noise. For this reason,

the ratio between the maximum peak amplitude and background noise was used as a measure of the level of dominance of a periodic phenomenon in all further analyses. The signal to noise ratio was proven to be a feasible analysis technique to compare the strength of instabilities despite varying measurement conditions.

3.3.3 Moving average RMS

To investigate the turbulent kinetic energy of a flow, all three flow components must be measured. The used setup limited the number of measurable components to two, so it was not possible to gain direct access to the total turbulent kinetic energy. However, particularly in the confined jet flow, it was of interest to obtain information about turbulence in the flow. Therefore, the Root Mean Square (RMS) of the obtained two flow components was determined only as shown in Equations 3.6 and 3.7.

$$RMS = \sqrt{\frac{1}{2}\overline{\left(v'_{axial}\right)^2} + \overline{\left(v'_{lateral}\right)^2}} \tag{3.6}$$

$$with \qquad v\left(t\right) = \overline{v} + v^{'}\left(t\right) \tag{3.7}$$

The described RMS value includes the axial and lateral components of the velocity fluctuations in the same way as the definition of turbulent kinetic energy, but without considering the third flow component. Although a flow is confined in the third component and has no average velocity, fluctuation velocities will be non-zero and isotropic turbulence cannot be assumed. However, the fluctuation energy in a confined flow component is significantly lower than in axial and lateral components, and is not expected to add any information of interest to the evaluation. Therefore, the RMS value was assumed to be representative of the overall turbulent kinetic energy in the liquid flow of the jet in Paper II.

In flow configurations with an instationary flow, the time-dependent average velocity must be considered when determining fluctuating velocities $v^{'}$. A similar problem occurs when a flow is dominated by a large-scale periodic phenomenon. An overall time-averaged mean value would produce large fluctuation velocities, and, consequently, high RMS values. To avoid artificially high RMS values, a moving average was applied as a contrast to an overall average. The moving average was calculated in blocks of constant time. The frequency of a large-scale periodic instability could be determined with the Lomb spectrogram, and a block size could be chosen. A block size of 0.25s was chosen for the confined jet, because the frequency analysis showed that it would be a good compromise between filtering large-scale movements and mapping turbulent kinetic energy.

3.3.4 Integral length scales

A turbulent flow can be characterized by the different length scales of the flow. Small length scales, such as the Kolmogoroff length scale, describe the size of the smallest eddies before they dissipate into heat due to viscosity. These small length scales are of importance when modelling a turbulent flow and when studying the dissipation rate of turbulent energy. The present study focuses on the interaction between comparably large particles and a fluid. Large and heavy particles are not influenced by the small eddies of a flow, but rather by flow instabilities and large-scale vortices. Therefore, it was of interest to study the Taylor macro scale Λ (Taylor [29]), i.e. the size of the eddies carrying the most energy.

$$\Lambda = v_{convective} \int_0^\infty R(\tau)\ d\tau \tag{3.8}$$

$$R(\tau) = \frac{1}{v^{'}(t)^2} \int_0^\infty v^{'}(t)\, v^{'}(t-\tau)\ dt \tag{3.9}$$

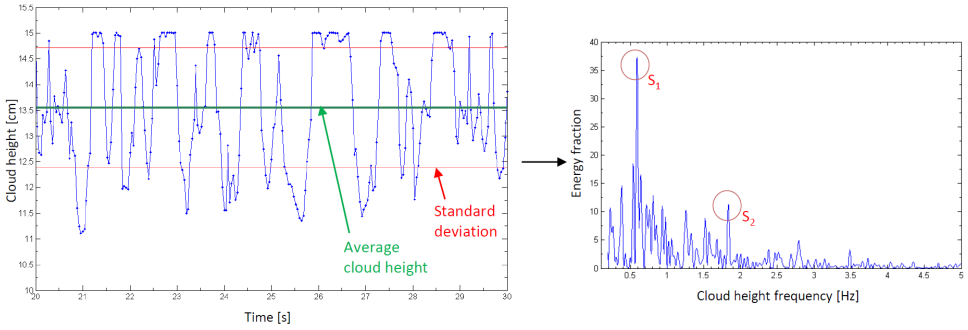

Figure 3.7: Determination of average cloud height, standard deviation and spectra

The method for directly determining the integral length scale (equ.3.8) would make use of the spatial correlation, which would demand simultaneous measurements at different locations. This cannot be achieved with the used setup. With the LDV technique, however, one-point measurements of two flow components with a very high temporal resolution can be obtained. Therefore, the calculations here are based on the temporal autocorrelation (equ.3.9) at each point to determine the Eulerian integral time scale, which multiplied by convective velocity gives the integral length scale Hinze [18].

3.3.5 Cloud height tracking

Two methods were developed to analyse the particle cloud in the suspension. Method A was specifically designed to directly track cloud height. It was possible to directly track cloud height at different locations and at every time step of the video (30s/25fps). For a certain horizontal coordinate, the Matlab algorithm evaluates and counts the pixels in the vertical direction and identifies the position at which a particle cloud surface can be identified. This was repeated for each frame in order to analyse temporal variations. The pixel counting process is visualised in Figure 3.8 with the symbol A.

The algorithm counts pixels from the top of the vessel downwards until a cloud

surface has been identified. To minimize error and false detection of single particles or dust, the cloud surface is defined with a threshold of 200 detected non-black pixels (16.7mm) in a row. If detected, the 200 pixels are subtracted again and the exact instantaneous cloud height value is stored.

Figure 3.7 shows a typical time chart of particle cloud height, as obtained with the described method. With these data it is possible to identify the average cloud height for a chosen location, as well as the temporal standard deviation. These values can be compared for different particle sizes and concentrations, as well as between different locations in the vessel used (Fig. 5.11). The collected data are also suitable for analysis with the Lomb algorithm (3.3.1). With the resulting spectra (Fig.3.7), it is possible to determine dominant periodic effects in the variations of cloud height. Locations close to the windward side of the baffles (left in Fig.3.8), similar to the evaluations of #010-#018 (Fig.3.1) in Paper I, were evaluated for cloud height dynamics. A few tests were conducted on the leeward side of the baffle (right in Fig.3.8), in order to show the spatial variation of particle cloud height (Fig.5.11).

3.3.6 Particle concentration tracking

Method B was designed to analyse variations in the local particle concentration at a certain position. The same video frames were used for this method. A square cell of the size of 200x200 pixels (16.7mmx16.7mm) was defined in the frame (the location of evaluation) and the algorithm determined the total pixel brightness in this cell. The value was stored and the algorithm was repeated for every frame of the video (time steps). Figure 3.8 shows a schematic view of both evaluation methods. The resulting data are a temporal variation of the brightness in the evaluated location; however, because the frame originates

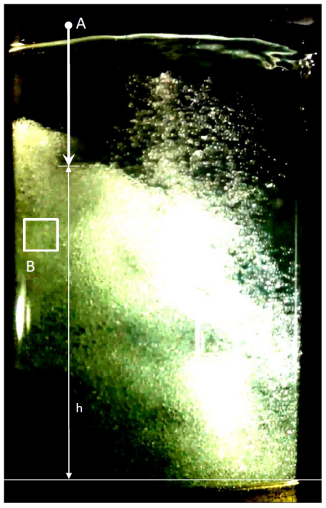

Figure 3.8: Cloud height and particle concentration tracking method

from particle reflections, it can be interpreted as a temporal variation of local particle concentration. It was not possible to determine a reference case, that is why only information on relative variation could be collected. This was sufficient in order to evaluate spectral data and to identify dominant periodic behaviours. The advantage of this method is, that it is possible to determine periodic behaviour also further down inside a particle cloud. Of course the video data still only captured the front facing view of the vessel and no information from inside the vessel could be obtained. The method was applied to 9 cells covering a region of 50x50mm at a vessel height of z=75-125mm ($1/2H-2/3H$).

3.4 Experimental procedures and cases studied

3.4.1 Paper I

In addition to a single-phase case, suspensions with particles of different sizes and concentrations were investigated. Water was used in all cases as the liquid phase and spherical glass particles with a density of 2.5kg/dm3 were used as the solid phase. Particles with a diameter of 1mm, 1.5mm and 2mm were used in

separate studies, the concentration was stepwise raised in order to investigate 17 different volumetric concentrations between 0%vol and 11.8%vol. The particle Stokes number, as a relation between particle relaxation time and the time scale of the instability, is shown in 3.1. Due to the decrease in penetration depths for the laser beam at high concentrations, it was only possible to conduct measurements up to 7.4%vol at positions deep in the vessel, #001 - #009 (Fig. 3.1).

The impeller speed was not changed during this study, and in all setups the suspension was agitated with 1800rpm(30rps). A high rotational velocity was needed to lift the particles off the bottom of the vessel. The criterion by Zwietering [7] for particle suspensions confirmed the visual observations that 30rps were sufficient for all suspensions except the highest concentrations of the 1.5mm and 2mm particles, where 34rps were needed. At these concentrations, stagnating particles could be observed at the bottom of the vessel and on the windward edge between the baffles and vessel wall.

The LDV apparatus was operated in single-burst mode and, for each position, a constant amount of 200,000 samples was acquired. The signal gain was set to 44dB and the high voltage to 1,216V. The laser power was varied to keep the data rate as stable as possible for all measurement conditions, however, a drop in the data rate was inevitable with a higher solid loading. The change in data rate caused a change in data acquisition time, which varied between 71.4s and

particle diameter in mm	particle relaxation time in s	reciprocal of MI frequ. in s	Stokes number
0.5	0.078	0.5618	0.139
1	0.156	0.5618	0.278
1.5	0.351	0.5618	0.625
2	0.624	0.5618	1.111

Table 3.1: Stokes number of different particles in relation to the identified MI

2,000s, relating to 127 and 3,560 periods of the determined MI phenomena.

3.4.2 Paper II

In the study of particle influence on the turbulence structures in a jet, suspensions with three different kinds of particles were investigated. In all suspensions, water was used as the liquid phase and solid glass particles with a density of 2.5kg/dm3 were used as the solid phase. The smallest particles had a diameter of 0.5mm, the bigger ones 1mm and the largest particles 2mm. Different volumetric concentrations of solid particles were investigated; the maximum concentration was 6.3%vol for the 1mm particles and 2.5%vol for the 0.5mm particles. To obtain the particle concentration in a jet, a sample was taken from a valve in the inlet pipe. The total weight of the sample was compared to the weight of the solid phase after vaporizing all water. The concentration was calculated in volumetric units independent of particle size.

The velocities of the liquid phase in the axial and lateral directions were measured with the two-component LDV apparatus. To obtain information about the average velocity, turbulences and large-scale instabilities, measurements were sampled for 120s at each location. The measurement locations were organized in eight horizontal lines at increasing distance from the nozzle. All lines

	2.5%vol	5%vol	7.5%vol	10%vol	15%vol	20%vol
0.5 mm	20	20	25	25	27.5	–
	25	25	27.5	27.5	30	–
	27.5	27.5	30	30	32.5	–
	30	30	32.5	32.5	35	–
1 mm	20	20	25	25	27.5	30
	25	25	27.5	27.5	30	32.5
	27.5	27.5	30	30	32.5	35
	30	30	32.5	32.5	35	37.5
2 mm	20	20	25	25	27.5	30
	25	25	27.5	27.5	30	32.5
	27.5	27.5	30	30	32.5	35
	30	30	32.5	32.5	35	37.54

Table 3.2: Experimental setup for particle cloud investigation (values of impeller speed in Hz)

were located in the centre plane of the tank. The measurement locations are further described in Figure 3.2. With the eight different lines, the profiles of velocity, RMS and integral length scale could be determined.

3.4.3 Paper IV

The experimental investigation of a particle cloud was conducted with particles of three different sizes (0.5mm/1mm/2mm), with average volumetric concentrations between 2.5%vol and 20%vol and with impeller speeds between 20Hz and 37.5Hz. This resulted in 68 different configurations (Table 3.2). In this way, all regions of solid-liquid mixing could be covered from a fully dispersed flow to an overloaded flow with an incomplete off-bottom suspension. All measurements were done at steady state conditions, meaning that the mixer start-up phase was not investigated. Particle concentration and impeller speed were gradually increased, and measurements were only initiated after mixing conditions had reached steady-state.

4

Mathematical modelling and numerical methods

4.1 Large Eddy simulation

The aim of the numerical study was to investigate the continuous and suspended phases in solid-liquid suspensions. The ability of the simulation to capture dominant periodic phenomena in a flow and in particle cloud formation was evaluated. The results from the numerical model were compared to experimental data (Paper I and Paper IV). Different turbulence models were tested for their ability to model the described problem. Simulations using less complex turbulence models, such as $k-\epsilon$ or $k-\omega$ models are not able to capture flow structures other than the time averaged flow field. Their averaging effect is too strong and most time-dependent information is lost. Reynold stress models (RSM), in contrast, are second-order closure models in which the eddy viscosity approach has been discarded and the Reynold stresses are directly computed. It was found that simulations using the RSM approach delivered a very stable flow field, which was similar to the results from the $k-\epsilon$

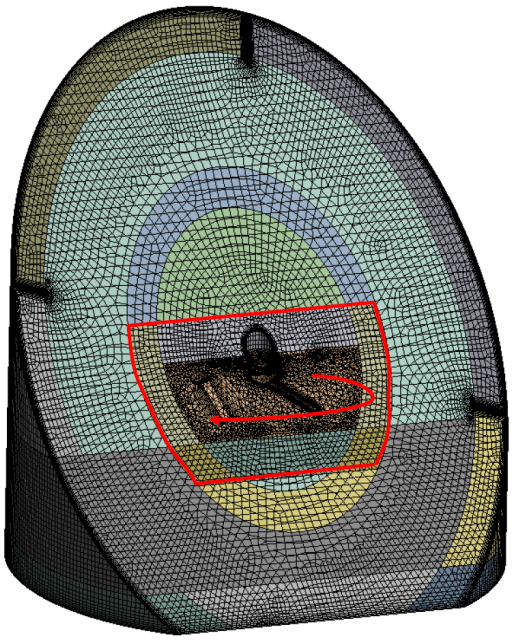

Figure 4.1: Multizone mesh with rotating impeller volume

model. After a comparably long additional simulated time (60 impeller rotations=2s) it could be observed that flow disturbances slowly grew and that the impeller discharge showed periodic fluctuations. Flow instability grew slowly throughout the whole vessel. Analysing the spectrum of the flow showed that the frequency of the dominant fluctuation was 3.7Hz, which is a significantly higher frequency than the experimentally determined 1.78Hz. Reynold stress models do not resolve smaller scale fluctuations, and it was concluded that the interaction between smaller turbulent structures could not be neglected in the calculation of large scale instabilities.

Consequently, LES was used in the subsequent calculations. In LES models, the flow field is decomposed into resolved flow structures and subgrid structures. All larger structures are directly computed, while structures smaller than the subgrid filter length scale are modelled with a corresponding subgrid model (Pope [30]). The Taylor microscale (λ) describes the inertial sub-range of the

turbulence energy cascade and serves as a reference length scale to determine the subgrid filter. Turbulent eddies in and below the inertial sub-range are isotropic, and can be modelled well. The structures down to the subgrid filter must be resolved in time and space, which demands a fine mesh and small time steps. Eddies with scales smaller than the grid were filtered out with the filtering process, which for a scalar Q was defined as

$$\bar{Q}(x) = \int_{\Omega} Q(x') G(x, x') dx' \tag{4.1}$$

where Ω is the fluid domain and G is the filtering kernel. The LES flow equations are assembled from the filtered continuity and filtered momentum equations:

$$\frac{\partial \bar{u}_i}{\partial x_i} = 0 \tag{4.2}$$

$$\frac{\partial \bar{u}_i}{\partial t} + \frac{\partial}{\partial x_j}(\bar{u}_i \bar{u}_j) = -\frac{\partial \bar{P}}{\rho \partial x_i} + \frac{\mu}{\rho} \frac{\partial^2 \bar{u}_i}{\partial x_j \partial x_j} - \frac{\partial \tau_{ij}}{\partial x_j} \tag{4.3}$$

where $\tau_{ij} \equiv \overline{u_i u_j} - \bar{u}_i \bar{u}_j$ denotes the subgrid-scale stresses, which requires a closure model. In this study, the subgrid scale stresses have been modelled using the Smagorinsky approach (Lilly [31] and Smagorinsky [32]):

$$\tau_{ij} - \frac{\tau_{kk}}{3}\delta_{ij} = -2\mu_t \bar{S}_{ij} \tag{4.4}$$

$$\bar{S}_{ij} = \frac{1}{2}\left(\frac{\partial \bar{u}_i}{\partial x_j} + \frac{\partial \bar{u}_j}{\partial x_i}\right) \tag{4.5}$$

$\bar{S}_{ij}$ is the filtered rate of strain tensor and μ_t is the subgrid scale turbulent viscosity which is modelled following the Smagorinsky-Lilly model (Lilly [31] and Smagorinsky [32])

$$\mu_t = \rho C_S \Delta^2 \left|\bar{S}\right| \tag{4.6}$$

where $\left|\bar{S}\right| = \sqrt{2\bar{S}_{ij}\bar{S}_{ij}}$ is the magnitude of the filtered strain rate and Δ is the local grid scale. In the dynamic Smagorinsky-Lilly model, the constant C_S , is dynamically computed based on the scales of motions in the resolved flow (Lilly [33]). For the spatial momentum discretization, a bounded central differencing scheme has been applied, the pressure discretization is of second order and for the transient formulation a bounded second-order implicit discretization scheme has been used.

All simulations were conducted on a computer cluster built on AMD Opteron 6220 CPUSs with 16 cores and 32 GB of RAM per node. The scalability of the model showed that it was not useful to use more than one node at a time; consequently, the calculations were conducted in parallel on 16 cores. Each case required approximately 30,000 core hours, resulting in 150,000 core hours for all five cases.

4.1.1 Mesh

The geometry for the numerical model was based on the experimental setup in Paper I and Paper IV. The dimensions and shape were identical to the vessel and the axial pitch-blade impeller in the experimental configurations (Fig.3.1). The model was split into 25 parts consisting of hexahedral cells, while the volume closest to the impeller had to be meshed with tetrahedal cells (Fig.4.1). The baffles were like solid walls without thickness, but because the impeller was expected to have a larger impact, it was modelled in full detail. Towards all surfaces, including the baffles, a boundary layer inflation

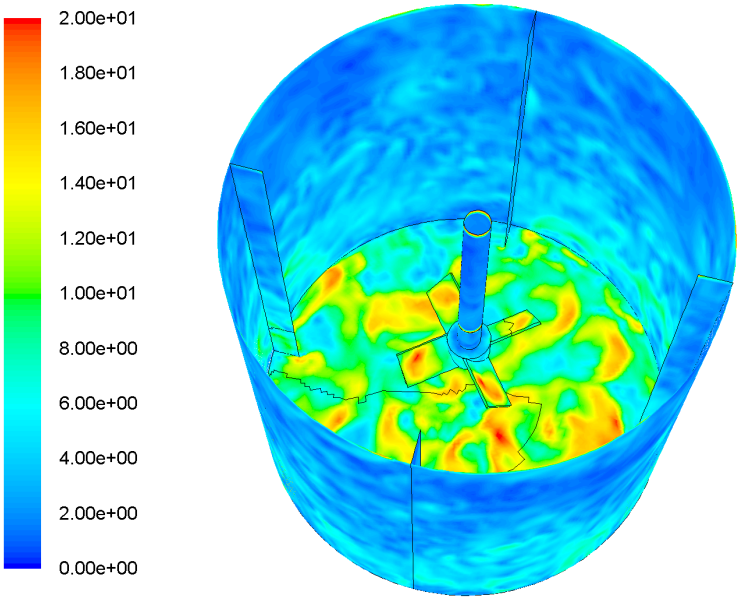

Figure 4.2: Turbulent wall-y+ values in the vessel

was considered. Figure 4.2 shows the turbulent wall-y+ on the walls in the vessel model. The impeller rotation was solved with a rotating mesh approach, in which a certain zone around the impeller was rotated against the stationary mesh containing the walls and baffles. The rotation of the rod was modelled as a moving boundary.

The cell size and the resulting filter length scale together with the time-step resolution are crucial to the application of a large eddy simulation. The solver uses an implicit filtering, which filters the turbulent scales dependent on grid scales. It is recommended that the subgrid filter length is equal to or smaller than the Taylor microscale λ of the flow:

$$\lambda = \sqrt{10\nu\frac{k}{\varepsilon}} \tag{4.7}$$

In order to find an appropriate grid resolution, simulations using an RSM were conducted to estimate the values of turbulent kinetic energy, the length scales

of the inertial subrange (λ) and related turbulent time scales (Δt):

$$\Delta t = \frac{\lambda}{u} \tag{4.8}$$

The predictions of the Taylor microscale (λ) were used to estimate the mesh size needed to resolve turbulent structures down to the inertial subrange. The ratio between the turbulent kinetic energy (k) and the dissipation rate (ϵ) is significantly smaller in the discharge of a jet, giving shorter time and length scales in that region. It was found that the Taylor microscale varied between 1.6mm and 0.2mm, and the corresponding time scale varied between 0.2s and 3*10-5s. Further LES simulations showed that a time step of 2*10-5s produced stable simulations and a steady convergence for all studied cases. The simulations converged after approximately 18 iterations per time step.

The small time-step size required to resolve turbulent structures with LES and the large time-scale of flow macro instabilities causes the simulations to be very time consuming. To guarantee a reliable frequency analysis, it was deemed necessary to simulate at least 4.5s (135 impeller revolutions), which resulted in 225,000 time steps. The frequency spectra were tested for different total simulation times and the amplitude and frequency became independent of the total simulated time as early as $t \geq 2.5s$. The final mesh contained 1,151,463 cells with an average subgrid filter length of approximately 1mm. Regions in the bottom third of the vessel, in the impeller discharge and in the direct vicinity of the impeller were each resolved in more detail.

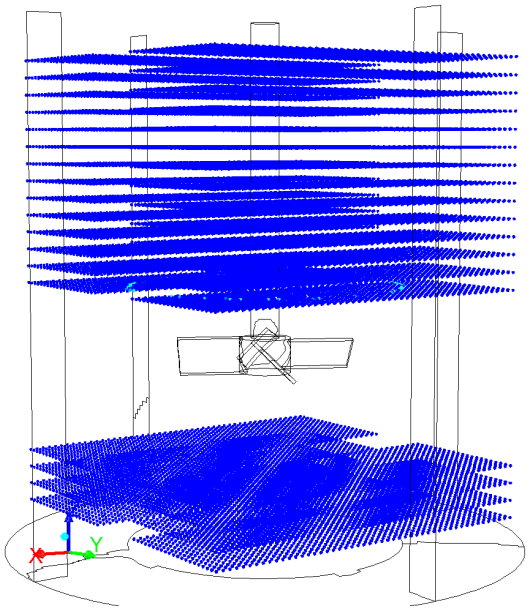

Figure 4.3: Injection of 37,800 particles into the vessel

4.1.2 Discrete particle model

A four-way-coupled Lagrangian particle model was used to simulate the solid phase of the suspension being studied. The fluid was simulated using an Eulerian approach, while the solid phase was simulated as a discrete phase model using a Lagrangian approach. In the Discrete Phase Model (DPM), each particle was simulated as a point mass and the trajectory was calculated using a force balance (Eq.4.10) that acted on the particle (one-way coupling). The particles were tracked with fluid flow time steps and an implicit tracking scheme was used. The momentum transport from fluid to particle is described by the drag force (Eq.4.11). The drag coefficient was modelled with a spherical drag model (Eq.4.12), where a_1, a_2 and a_3 were constants that applied over a wide range of Re as given by Morsi and Alexander [34]:

$$\frac{du_p}{dt} = F_D\left(u - u_p\right) + \frac{g_x\left(\rho_p - \rho\right)}{\rho_p} + F_x + F_G \tag{4.9}$$

$$F_D = \frac{18\mu}{\rho_p d_p^2}\frac{C_D Re}{24} \tag{4.10}$$

$$Re = \frac{\rho d_{\prime p}\left|u_p - u\right|}{\mu} \tag{4.11}$$

$$C_D = a_1 + \frac{a_2}{Re} + \frac{a_3}{Re^2} \tag{4.12}$$

The influence of each particle on the fluid phase was simulated with a source term in the Navier-Stokes equation, representing the momentum exchanged from particle to fluid (two-way coupling). The source term is usually only active in the centre of each particle and only affects the computational cell that holds this centre of the particle. Therefore, the particles must be smaller than the cell size. The small subgrid filter length scale required by the LES model created a dilemma concerning the cell size of the model. For this reason, a node-based averaging model with a Gaussian averaging kernel (Gaussian factor=0. 5) was selected to average the DPM source terms and to distribute the effect to neighbouring cells (Apte et al. [35]).

The DPM model does not consider any displacement of fluid, because the particles do not have any actual volume. In the same way, they can also take up the same position or fly through each other. To prevent the endless agglomeration of particles on the vessel bottom or at stagnation points from happening, a collision model must be applied. A Discrete Element Method (DEM) collision model was used to simulate zones of high particle concentrations and particle-particle interaction (four-way coupling). An adaptive collision mesh width with an edge scale factor of 1.5 was used in the DEM collision model. Particle-wall collisions (walls, baffles and impeller) and particle-particle collisions were sim-

ulated using a spring-dashpot model for normal forces and a Coulomb friction model for tangential forces. The small time-step size of the simulation was very useful for the computation of the collision model, since the maximum overlap between particles at collision and the total number of collisions could be kept within a reasonable range.

$$\kappa \geq \sqrt[3]{\frac{2V^2}{e_D^2 3\pi} D\rho} \tag{4.13}$$

The spring constant (κ) was estimated using Equation 4.13, where D is the particle diameter, ρ is the particle density, ϕ is estimated as the maximum relative velocity between the two collision partners and e_D is the estimated fraction of diameter for allowable overlap.

The coefficient of restitution describes the amount of energy recovered from the collisions; it was set at 0.95 for all inter-particle as well as the particle-wall collisions.

The simulation was computed until single-phase steady state was achieved before any particles were injected. Early tests have shown that the injection of particles with an initial velocity cause convergence problems due to strongly increased momentum in the vessel and could cause unphysically strong collisions with each other. For this reason, it was decided to inject each particle in a unique location without any initial momentum (4.3). The simulation was computed until a mixed steady state of the solid-liquid suspension was achieved. Data collection was started only after steady state conditions were achieved. The integral of the wall shear stresses on baffles and walls, as well as the volume fraction of the discrete phase in the bottom third of the vessel, were monitored in order to determine the initial single-phase steady state as well as the mixed steady state of the suspension.

4.2 Data evaluation and cases studied

The subgrid-scale model can only model turbulence in the inertial subrange and lower. From the energy distribution of turbulent length scales it follows that at least 80% of the turbulent kinetic energy must be directly resolved (k_{res}) and only 20% is contained below the inertial range (k_{sts}). It is, therefore, recommended to evaluate the resolved turbulent kinetic energy ratio (k_{ratio}) of an LES simulation in order to test the validity of the applied model:

$$k_{res} = \frac{1}{2}\left(\overline{(u'_x)^2} + \overline{(u'_y)^2} + \overline{(u'_z)^2}\right) \tag{4.14}$$

$$k_{ratio} = \frac{k_{res}}{k_{res} + k_{sts}} \tag{4.15}$$

In all investigated cases an average of 90% of the turbulent kinetic energy was resolved, which is well above the recommended 80% (Pope [36]). The value for k_{ratio} varied in the vessel, the lowest identified value of approximately 70% could be found in the high turbulence zone of the impeller discharge in the vicinity of the impeller. In this region, a refinement of the mesh would improve the solution for continuous-phase turbulence, but this would cause major problems with the discrete particle model.

4.2.1 Paper III - Mixing vessel

The flow conditions in the numerical model were intended to match the experimental study in Paper I, which was conducted with an impeller speed of

Particle diameter	Number of particles	volume concentration	mass concentration	critical impeller speed (Zwietering [7])
1 mm	18,900	0.4%vol	1%w	18.91 Hz
1 mm	37,800	0.75%vol	2%w	20.52 Hz
2 mm	9,450	1.5%vol	3.9%w	25.79 Hz
2 mm	18,900	3%vol	7.8%w	28.22 Hz

Table 4.1: Setup for numerical simulations for MI investigation

30Hz (1800rpm) and with water as the continuous phase with a density of $998.2 kg/m^3$. The solid particle phase was modelled to match the experiments in Paper I with solid glass particles with a density of $2,600 kg/m^3$. The four different investigated suspension setups are described in Table 4.1.

In each of the simulated time steps ($\Delta t = 2 * 10^{-5}$s), the velocity components of the continuous phase at the 18 locations were monitored and stored. The data collection locations were identical to the measurement locations in the experimental study (Fig. 3.1). The time-dependent velocity data from the simulations were evaluated using the same Lomb-algorithm as used for the experimental data analysis (Chap. 3.3.1 and Fig. 3.6).

The obtained spectra were analysed with respect to the frequencies of dominant periodic phenomena in the flow. The frequency and amplitude of the periodic phenomena were compared between the different suspensions and to the findings from the experimental study.

4.2.2 Paper IV - Particle cloud

The numerical simulations for the study in Paper IV were intended to investigate the behaviour of the discrete particle phase. The continuous phase was modelled as purified water and the particles as solid glass. Two different impeller speeds ($30Hz$ and $20Hz$) were investigated. Table 4.2 gives an overview of the four simulated conditions.

The numerical simulations were conducted with time steps of $\Delta t = 2 * 10^{-5}$s,

Particle diameter	Number of particles	volume concentration	mass concentration	impeller frequency
2 mm	60,000	9.5%vol	24.3%w	30 Hz
2 mm	37,800	6.0%vol	15.5%w	30 Hz
1 mm	60,000	1.6%vol	3.0%w	30 Hz
1 mm	60,000	1.6%vol	3.0%w	20 Hz

Table 4.2: Setup for numerical simulations for cloud height investigation

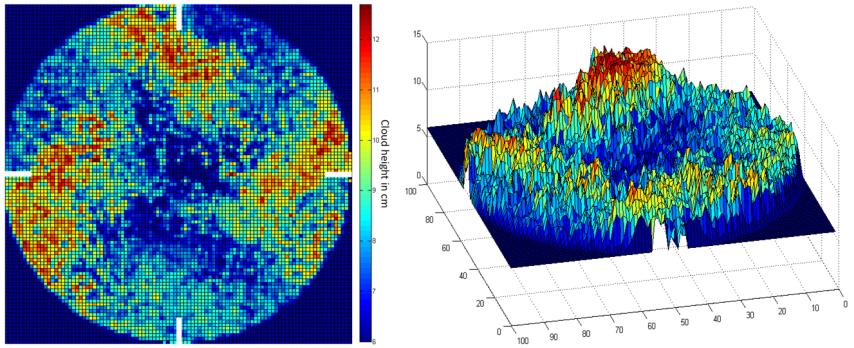

Figure 4.4: Particle cloud surface with CFD - 2mm 9.5%vol

but data were collected only every 100th time, resulting in a data rate of 500Hz, and a total simulated time of 5s. The coordinates and velocity components of each particle were exported to particle history data. In this way, it was possible to obtain information about the exact location of each particle in any of the collected time steps.

The post-processing of the collected data was done with an algorithm developed in Matlab. The additional methods for analysing the temporal behaviour of the particle cloud were similar to the ones developed for the experimental study in Paper IV (Chap.3.3.6).The particle cloud height was tracked by creating a vertical column of test cells. The number of particles contained in each of these cells was counted and the local particle volume fraction was determined. The location of the particle cloud surface was defined as the vertical location with the strongest gradient in particle concentration. By repeating the algorithm for each of the collected time steps, the temporal variation of cloud height could be captured. Any further data processing, such as average cloud height, standard deviation as well as frequency spectra could be determined in the same way as in the experimental cases (Chap.3.3.6 and 3.7).

The algorithm for detecting cloud surface can not only be used in one location in a vessel, but, rather, can be looped through the entire vessel. For this

reason, to detect the complete instantaneous cloud surface, the algorithm was conducted at 75x75 locations in the vessel. Figure 4.4 shows the resulting cloud surface in 3D and 2D. When conducting this algorithm throughout the vessel, the local volume fraction of solid particles could be determined for the entire vessel and could be analysed (Fig. 5.14).

5

Results and discussion

5.1 Paper I

The velocity measurements conducted in the mixing vessel showed the strongest periodic behaviour. Tests at different impeller speeds were conducted and a linear relation between the dominant frequency peak and impeller speed could be confirmed (Table 5.1). The non-dimensional frequency was identified as Strouhal=0.06. At an impeller speed of 30Hz this led to a frequency of 1.78Hz, which was identified as an MI phenomenon (Table 5.1). The measurements were taken at 18 different locations in the vessel (Fig. 3.1), and the Lomb spectrograms were analysed for all measurements. MI phenomena could be found in all measurements, but the strength of the phenomena varied between

impeller speed in rpm	impeller freq. in Hz	MI freq. in Hz	non-dimensional MI freq.	Re
390	6.5	0.381	0.059	18,000
1,050	17.5	1.06	0.061	49,000
1,500	25	1.5	0.060	70,000
1,800	30	1.78	0.059	84,000

Table 5.1: MI frequency with varying impeller speed

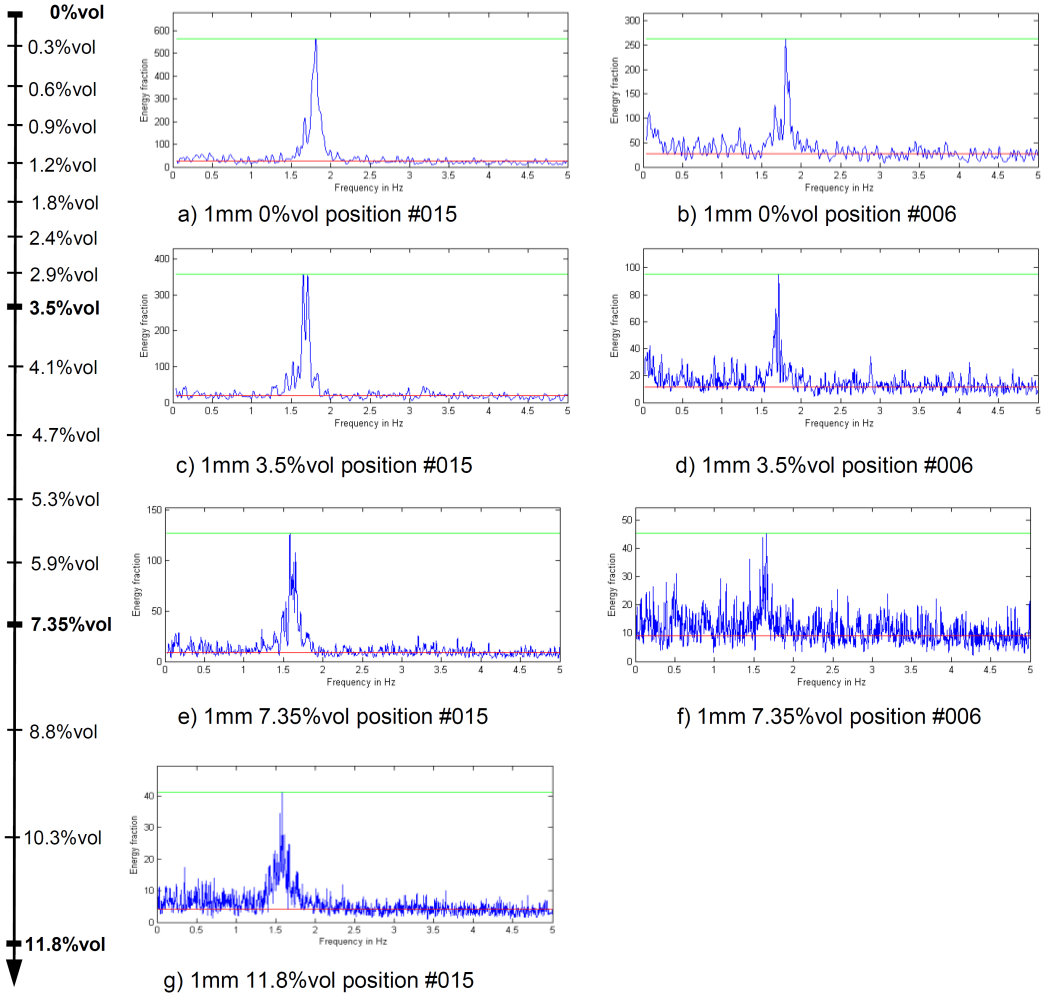

Figure 5.1: Lomb spectrograms for different locations in the mixing vessel by increasing particle concentration

different locations. At the locations #010-#018, on the windward side of the baffle, the strongest influence of MI phenomena could be identified. Suspensions at 11 different concentrations of particles of three different sizes were investigated in this study.

As mentioned in Chapter 3.3.2, it proved to be difficult to compare the strength of the MI phenomena between different setups at different locations in the vessel. Therefore, the ratio between the max amplitude of MI phenomena and background noise was used to determine the strength of the MI. A number

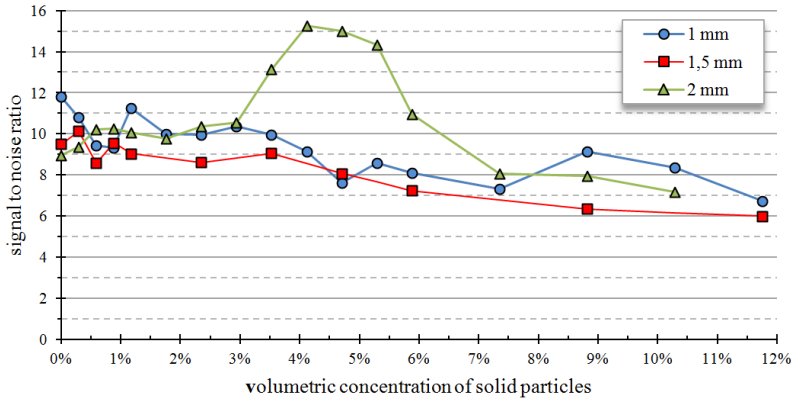

Figure 5.2: Amplitude of the MI with increasing particle concentration

of test measurements were conducted to inspect the stability of the measured results. The sensitivity of the analysis to variations of data rate, sampling time and number of samples was tested; the dependency of the results was also tested for different settings of the LDV technique, such as the oversize rejection value, the burst detection criterion or quality factor. It was found that the frequency of the MI phenomena was determined as Strouhal=0.06 under all conditions, but the maximum amplitude of the MI showed a certain sensitivity to the data rate and the total time of sampling. The signal-to-noise ratio, on the other hand, showed better consistency in determining the strength of the MI phenomena.

Figure 5.1 shows the Lomb spectrograms from the suspension with 1mm particles. One measurement position close to the baffle (#015) and one measurement position in the vessel bulk (#006) were chosen to be presented in the figure. The results are representative of all the other measurements. The single-phase case was re-measured for all three particles to rule out variations in the setup when changing the suspensions. At locations deep in the vessel, it was not possible to measure concentrations higher than 7.35%vol, while at the baffle, a concentration of 11.8%vol could be measured (Fig. 5.1). It can be seen that

the MI peak remains constant at the same frequency for all concentrations investigated. However, while the value of the frequency of the MI phenomena remained constant it was possible to identify a lower amplitude of the MI when the particle concentration was higher. Even though the strength of the MI phenomena decreased with increasing solid concentration, the MI could still be clearly identified at the highest measurable concentration.

The results obtained with the 1.5mm particles showed the same behaviour as the suspension with 1mm particles. The suspension with 2mm particles, on the other hand, did not show a constant decrease in MI strength, but rather an increase at moderate concentrations followed by a decrease. Figure 5.2 shows the signal-to-noise ratio of the MI with higher particle concentration. Each point in the chart was obtained by averaging over all 18 measured positions. Between 3%vol and 6%vol, the 2mm particle suspension was characterized by stronger MI strength than the single-phase case. The increase in MI strength was observed at all 18 positions, but was the strongest at the locations #015 - #017. The increase in MI strength coincided with the formation of a clear cloud height at 2/3 of vessel height. It was assumed that the different behaviour of the larger particles was related to the larger Stokes number. For the 2mm particles, a value of Stokes=1.1 was determined, while the smaller particles had values of 0.2 and 0.6 (Table 3.1). The cloud height quickly decreased to 1/2 of vessel height when the concentration was higher. The kinetic energy of the flow was not sufficient to lift all particles. The flow above the cloud was free of particles and nearly stagnant. The energy required to keep the particles afloat was taken from the fluid flow, so that the flow above the cloud appeared to be cut off from the mixing flow. The cloud height was not stationary, but was characterized by strong periodic fluctuations. Only the upwards jet from the windward side of the baffles (Figure 2.4) penetrated the cloud and transported

particles into the upper part of the vessel. The jet also periodically fluctuated in strength as part of an MI. The suspension with the larger particles had a strong abrasive behaviour. Significant abrasion occurred at the impeller blades and at the baffles due to collisions with particles.

Visual observations of the particle dispersion showed that collision behaviour of particles differs between more and less dense suspensions. In less dense suspensions, particles travel a far distance after a collision and disperse in the vessel. Especially collisions with the impeller blades and the vessel bottom cause a very strong rebound. Particles also collide with each other, and have enough space to travel a significant distance with post-collision trajectories. In more dense suspensions, the free space between particles is very limited. If the trajectory of a particle differs from the flow streamlines after a collision, it has no space to travel before colliding with another particle. The particle trajectories are less random and the particles move in a collective manner. In this way, the particles do not disperse in the same manner as in less dense suspensions. The particle flow is more homogenous and behaves like a continuum similar to dense granular flows. The flow of the particle phase is significantly influenced by the momentum transfer due to inter-particle collision.

5.2 Paper II

Different particle suspensions were investigated in a confined jet setup to study the effect of solids on turbulence structure and flow instabilities. The axial and lateral components of the fluid velocity were measured at 162 locations of the confined jet. Particles with a diameter of 0.5mm, 1mm and 2mm were used as the solid phase. The obtained flow profiles were analysed for axial velocities, RMS values as well as integral length scales and dominant flow frequencies.

The analysis of the single-phase jet clearly showed two regions of the jet. Close to the nozzle, where the jet was characterized by a stable shear layer and farther from the nozzle, where the instabilities dominated the flow. The jet became unstable after a distance of approximately 10 times the nozzle diameter (10*D). In this region, the flow was dominated by large-scale fluctuations with a low frequency. Figure 5.3 shows the Lomb analysis of the lateral flow component at the centreline positions. At short distances from the nozzle, the Lomb spectrograms only showed peaks at frequencies related to vibrations and the rotation of the screw pump. With greater distance, a strong peak at low frequencies was recognizable. The low frequency peak at 5Hz - 2Hz was the instability of the jet. The analysis of the axial flow component showed the same behaviour, but less pronounced due to high axial velocity. Frequency, spatial resolution and strength were the same for the single-phase jet as for the suspension with 0.5mm and 1mm particles. The 2mm particle suspension, on the other hand, showed greater stability in the jet. While the frequency remained the same, the strength decreased and the instability occurred at a greater distance from the nozzle.

Figure 5.4 shows the RMS profiles of the single-phase jet in a comparison between the three different particle suspensions. The shear-layer-dominated flow is clearly identifiable with the typical double peak, while the flow farther from the nozzle is characterized by flatter and wider profiles. The presence of the particles caused higher RMS values in the region close to the nozzle. The exchange of momentum in the shear layer and the jet core increased. The RMS profiles for the 2mm particle suspension do not go down to zero outside the jet, but rather show very high RMS values in regions where the average flow is already zero. This is caused by particles that leave the jet due to collisions and carry their momentum into the fluid bulk outside the jet. The 2mm particles

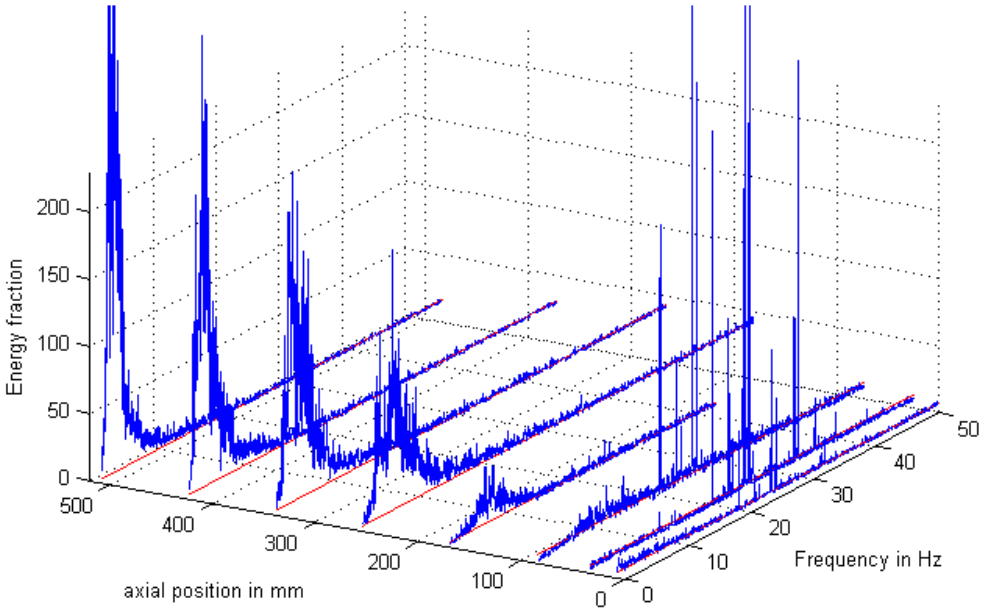

Figure 5.3: lateral Lomb spectrogram of centreline positions in single phase

are largely influenced by particle collisions and particle inertia. The 1mm particle suspension was measurable up to a concentration of 6.3%vol. Significantly higher RMS values closer to the nozzle were observed while the RMS profiles farther away from the nozzle were lower. This is in good agreement with the definition of the particle Stokes number in a jet by Hardalupas et al. [23] (Equation 5.1). With greater distance from the nozzle the particle Stokes number decreases and particles can better follow flow structures. Gore and Crowe [2] has described that large particles augment turbulence to the flow, while small particles attenuate turbulence. A variation of flow length and time scales also means that the same particle can be small in relation to the flow scales in one region and large in another. The integral length scales d_p/Λ (Equation 3.8) at the centreline positions increase linearly with the distance from the nozzle.

The values obtained in the measurements are in good agreement with the description by Wygnanski and Fiedler [19] of a gaseous jet. The presence of solid

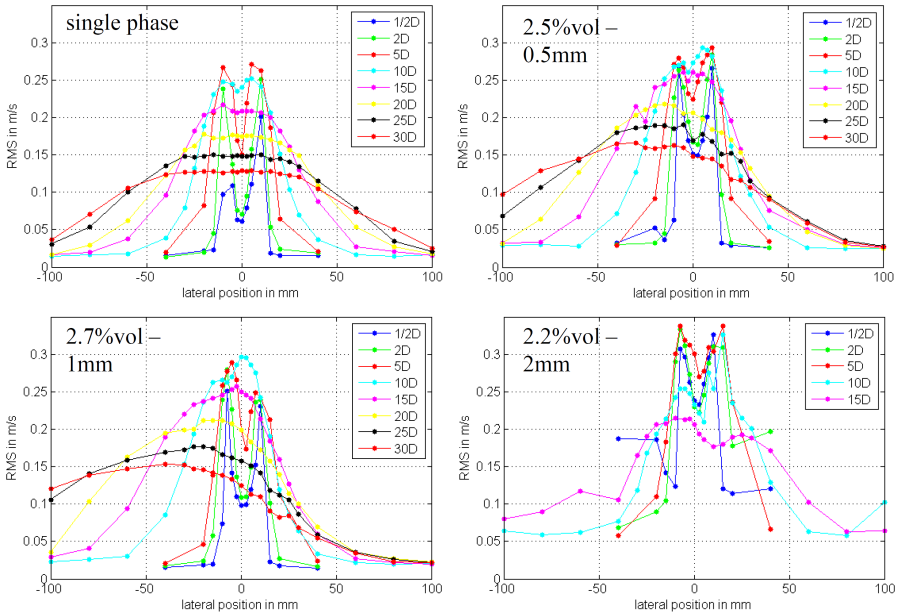

Figure 5.4: RMS profiles of suspensions with different particles

particles has only a minor influence on the integral length scales with no clear trend. For the 2mm and the 0.5mm particles, a slight decrease was found while the integral length of the 1mm particle jet was identical to the single-phase case. The profiles of the integral length scale have a shape similar to the RMS distribution. This is in good agreement with the findings of Benayad et al. [37], that the integral length scale is maximal in the shear layer.

$$S = \left(S_e \frac{1}{6.57} \left(\frac{x}{D} \right)^2 \right)^{-1} \tag{5.1}$$

$$S_e = \frac{D/U_0}{\tau_p} \tag{5.2}$$

The axial velocity profiles did not show any significant difference between the single-phase jet and the different particle suspensions. Figure 5.5 shows the axial velocity profiles of the flow with 2.2%vol of 0.5mm particles. The axial profiles did not indicate any change in the decay of the centreline velocity or

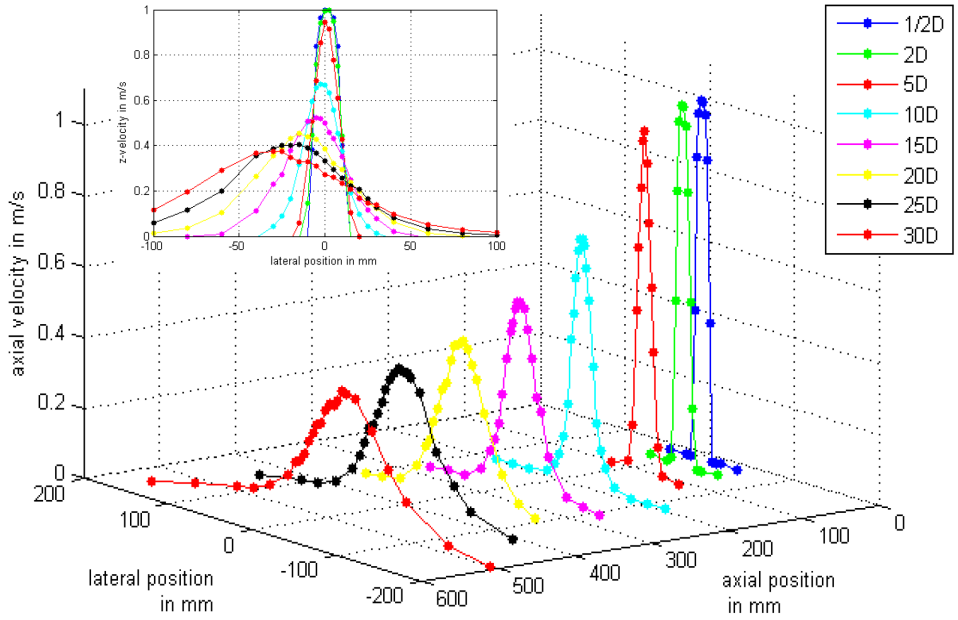

Figure 5.5: Axial velocity distribution at 2.2%vol of 0.5mm particles

any change in jet width. While the single-phase jet was stable at the centreline, a greater tendency to diverge from the centreline was observed in particle suspensions. The jet containing the largest particles, 2mm, did not show this behaviour and was stable at the centre position even at 4.5%vol. The 1mm particle flow only showed a minor tendency to diverge from the centreline and only at very high concentrations (higher than 4%vol). With the smallest particles, 0.5mm, the jet showed a strong tendency to leave the centreline position. With a higher solid concentration, the jet was more likely to diverge, which made it impossible to produce reliable measurements of concentrations exceeding 2.5%vol. The jet did not show a preferred direction, divergence to the right or to the left was equally as common. The cause of this phenomenon was most likely asymmetric disturbances inside the tank. While the single-phase jet remained stable, the particle suspension was more sensitive and enhanced the disturbance so that the jet diverged. Similar to the study with the mixing vessel, the particles ground the steel surfaces. Especially the largest particles

caused significant abrasion. This caused a problem with visibility due to steel dust in the suspension and made LDV measurements increasingly difficult.
Visual observations of the flow showed that the collision behaviour varied between different particles and different concentrations. Large particles featured strong collisions with post-collision trajectories which crossed the fluid streamlines. In the region close to the nozzle, this led to the effect that particles were transported out of the jet due to collisions in the jet core. Particles with a large Stokes number could be dispersed a far distance and, thereby, carry momentum into different flow regions. Smaller particles were more affected by the fluid flow, and were not able to travel longer distances against the fluid streamlines. Particle dispersion was mainly due to fluid vortices and less due to collisions.
The collision effects differed between more or less dense suspensions. In less dense particle suspensions, the particles could travel a farther distance after a collision before colliding again. After a collision, the two particles involved travelled into different flow regions and transferred their momentum to the fluid. In denser particle suspensions, the particles were limited in their freedom to move. A short time after a collision, they collided again and transferred their momentum to other particles. The overall particle flow was more homogeneous and all particles had more similar vectors than in less dense systems.

5.3 Paper III

The computational simulations using an LES turbulence model successfully simulated the flow structures in the mixing vessel. Figure 5.6 shows the instantaneous axial velocities in the mixing vessel under single-phase conditions. It

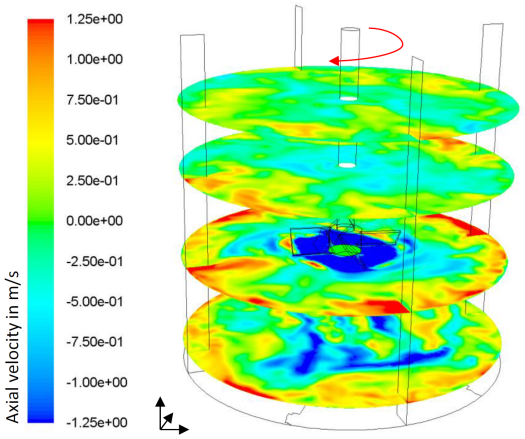

Figure 5.6: Instantaneous axial velocities in single phase mixing vessel

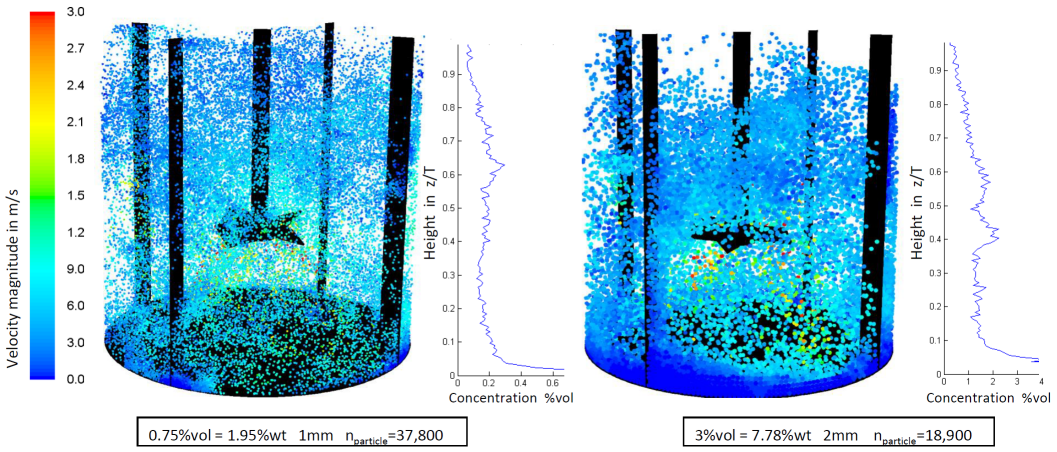

Figure 5.7: Simulated particle cloud of different suspensions

can be seen that the mixing flow was dominated by complex structures with strong temporal fluctuations and variations in flow orientation. The highest upwards flow (positive axial velocity) was found on the windward side of the baffle, and is known as a baffle jet (Jahoda et al. [12], Bittorf and Kresta [38]). These baffle jets are typical flow structures in mixing vessels and are of great importance for particle suspension, because flow particles can be carried into the upper regions of a vessel by high momentum.

The formation of a particle cloud could be modelled in the numerical simulation with the addition of particles. Figure 5.7 shows the simulated particle

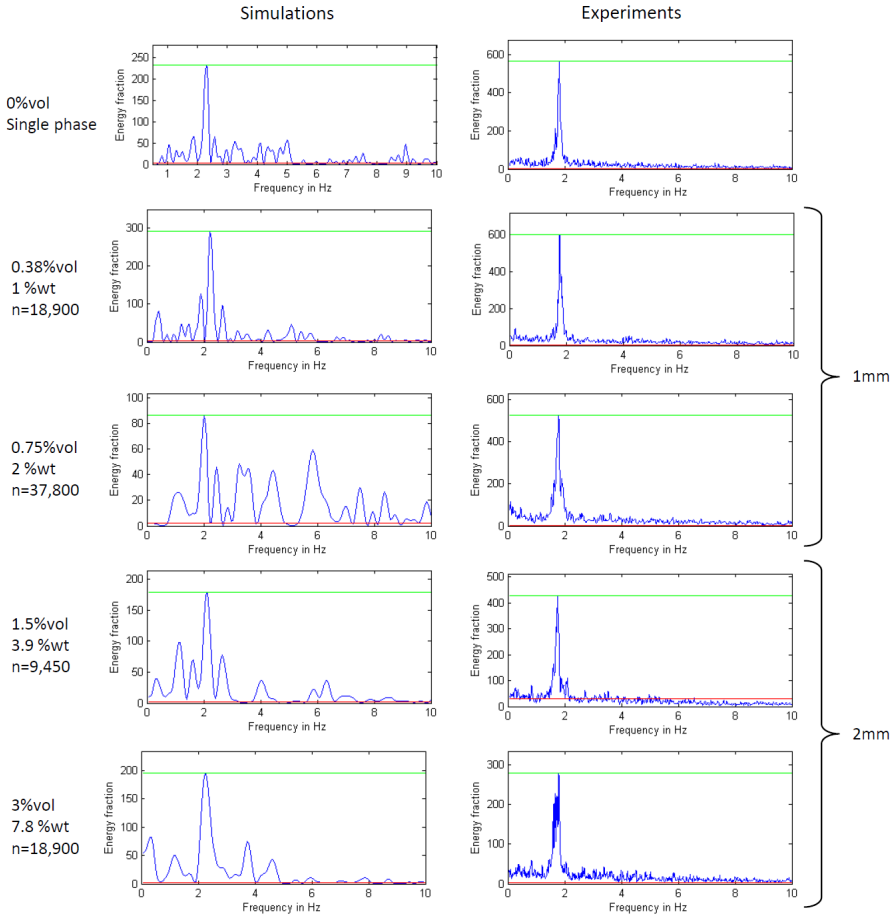

Figure 5.8: Comparison of energy spectra between CFD and experiments (location #016)

suspension with different particle sizes and concentrations. The particle concentration in the simulated vessel was determined by cutting horizontal slices out of the vessel and counting the particles in each slice. The vertical particle concentration is shown in Figure 5.7. It can be seen that a layer of high concentration was formed in the upper region of the vessel. This layer was formed by descending particles colliding with upwards flowing particles, and the particles in this region were nearly stagnant. The vertical position of this dense particle layer varied and was strongly affected by the strength of the baffle jets. The actual particle cloud height was closely related to the dense particle layer and fluctuations therein; it can be suggested that the dense particle layer is another

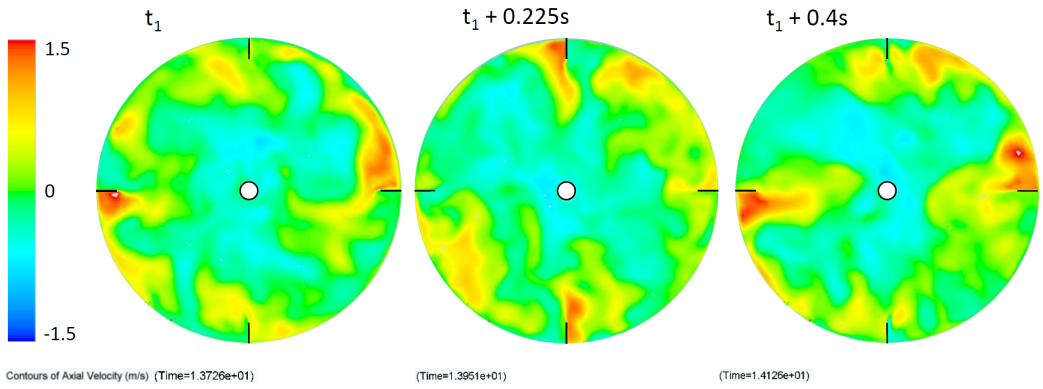

Figure 5.9: Axial velocities at different time steps in vertical plane

way of defining cloud formation.

The continuous-phase velocities were tracked at 18 locations (Fig 3.1) in the vessel. With these time-dependent data it was possible to apply the Lomb algorithm (Chap. 3.3.1). The resulting spectra gave information about the energy content of the periodic phenomena in the simulated flow. The bottom locations (#010 - #012) did not deliver any clear peak in the spectra. With increasing height, a clear peak was detectable at $f_{MI} = 2.2Hz$. Above one third of the vessel height ($1/3H$, equal to impeller height) the peak significantly dominated the spectra, which indicates that the periodic phenomenon with the frequency of 2.2Hz dominated the structures in the flow. The dominant peak was an order of magnitude slower than the impeller speed (30Hz with impeller passage frequency of 120Hz), and, therefore, has been characterized as a low frequency instability. The corresponding Strouhal number is $S_{MI} = 0.073$. Figure 5.8 shows a comparison of the spectra of the simulated flow case with the experimentally obtained spectra. Spectra from the location #016 (z=80mm) are shown and compared between different suspensions. It can be seen that the detected frequency is in good agreement, but slightly higher than the frequency in the experimental data ($f_{MI} = 1.78Hz, S_{MI} = 0.06$, Fig. 5.1). It can be concluded that the simulated flow experienced a dominant periodic instability

with the same frequency as the experimental vessel and that the same frequency could be detected in all the investigated suspensions. The difference in resolution in the spectra resulted from the different lengths of simulation time and differences in the sampling frequency between experiments and simulations. The amplitude-ratio between peak height and background noise was similar, but the exact quantitative evaluation of the energy fraction of the MI could not be achieved in all cases, especially the 0.75%vol 1mm ($n_{particle} = 37.800$) case lacks accuracy.

It could be observed that the baffle jets varied in strength; with phases of strong axial momentum alternately with phases of weak and nearly negative axial momentum. Figure 5.9 shows the axial velocity in a horizontal plane at 2/3H at different time steps. It can be seen that the strength of the baffle jets fluctuated periodically and appeared to migrate around the vessel. Observations found similarities to the periodic phenomenon described as macro swelling by Jahoda et al. [39] and the flow macro-formations by Bruha et al. [16]. By visual inspection of the time evolution of the flow field, a periodicity of roughly 0.4s could be identified, which is equivalent to a frequency of approximately 2.5Hz. The similarity to the MI frequency of 2.2Hz obtained with the Lomb algorithm is striking.

5.4 Paper IV

When investigating particle cloud dynamics, it can be seen that a particle cloud is characterised by strong temporal and spatial variations. At one instant in time, the cloud height will be strongly different at different locations in a vessel. If one location is observed throughout time, strong variations of particle cloud

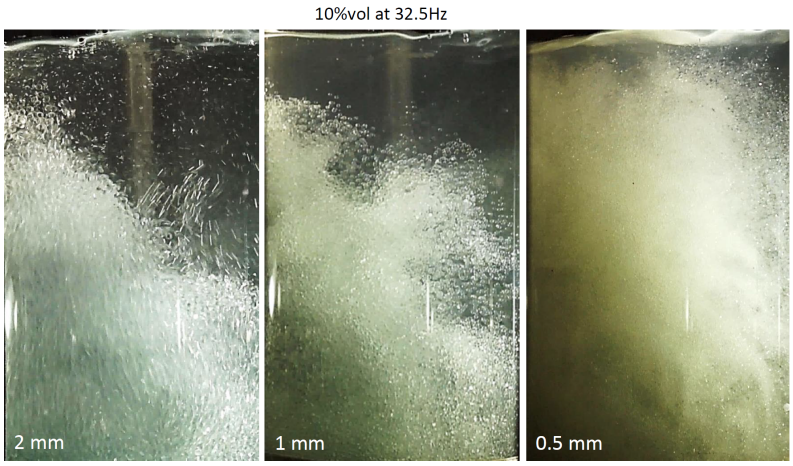

Figure 5.10: Particle cloud of suspensions with different particle sizes

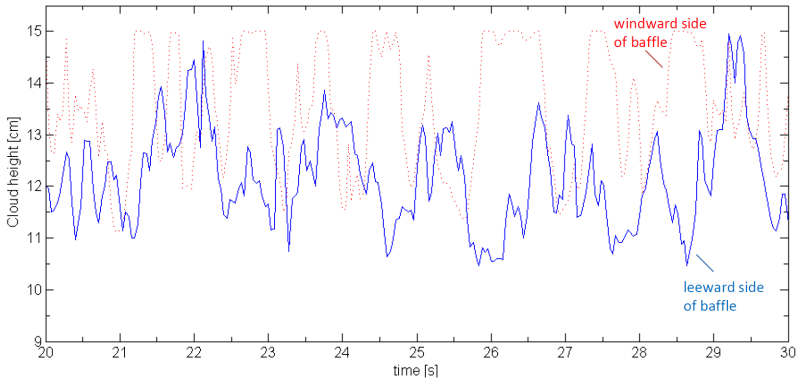

Figure 5.11: Temporal variation of particle cloud height at two different locations in the vessel

height can be found. Figure 2.6 summarizes this behaviour by describing the temporal variation at two different locations in the vessel. This agrees well with the results from cloud height measurements at two different locations shown in Figure 5.11. The temporal average cloud height will be different for the two locations. It could be observed, however, that temporal variations in the vessel behaved with the same frequency, but phase-shifted. This is due to the fact that the spatial average at any time step of the cloud height is nearly constant; it appears as if the cloud fluctuates, but the average does not move up or down.

With the cloud height tracking method (Chap. 3.3.5) it was possible to identify

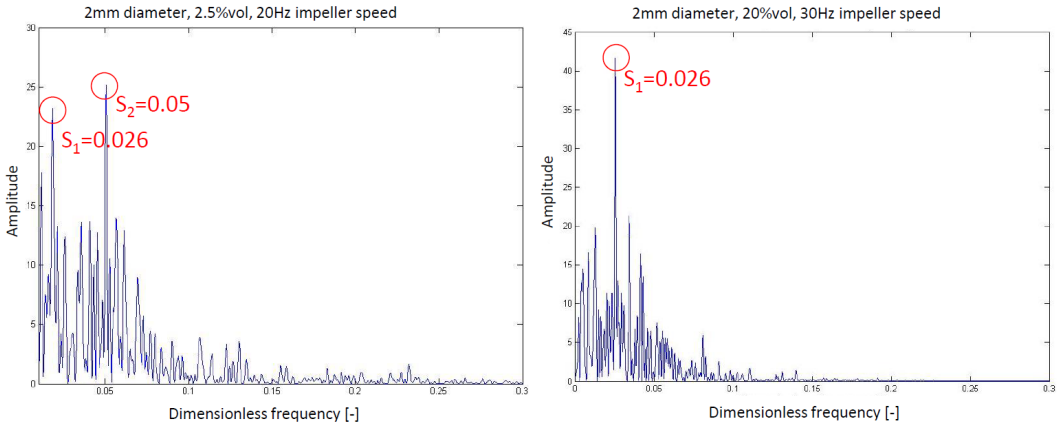

Figure 5.12: Spectra of cloud height analysis at different concentrations (2mm 2.5%vol and 20%vol)

the time-averaged cloud height and the standard deviation in time (Fig. 3.7). It could be seen that the average cloud height increased linearly with impeller speed and decreased linearly with a larger volume fraction of particles. Smaller particles formed clouds with a higher average cloud height than larger particles. The temporal variation of the identified cloud height was significantly less than for larger particles, this could be seen when analysing the standard deviation, which was smaller for small particles. This data evaluation only considered the exact detected cloud height, when analysing the particle concentration gradient in detail, it could be seen that large particles formed a significantly stronger concentration gradient, meaning that the particle cloud was very well separated from the clear liquid layer. Smaller particles formed less well-defined particle clouds and it was more likely that a particle was present outside of the cloud. Figure 5.10 shows the dispersion of a particle cloud with different-sized particles (2mm/1mm/0.5mm). Smaller particles were more dominated by drag than inertia. This characteristic increases their ability to follow small-scale turbulence vortices and, therefore, they are more likely to be randomly dispersed. Larger particles are more dominated by the mean flow field and macro-scaled

low-frequency phenomena.

The spectral analysis with the Lomb algorithm provided information about the energy content of each frequency in cloud height data (Fig. 3.7). Strong peaks in the spectra indicate significant periodic phenomena in the flow. Most observed cases showed more than one strong peak in the spectrum, and each peak was not always clearly distinguishable. Nevertheless, two reoccurring dominant peaks were outstanding in nearly all cases. It could be observed that the frequencies of these peaks were linearly related to impeller frequency, and, therefore, can be described with a constant Strouhal number. The lower of the two dominant frequencies was consistently identified in the frequency regime of $S_1 = 0.02 - 0.03$, the higher frequency occurred between $S_2 = 0.05 - 0.06$. Roussinova et al. [40] and Galletti et al. [11] have identified two dominant MI frequencies in a single-phase vessel at $S_{MI} = 0.015$ and $S_{MI} = 0.065$. This is similar to the S_1 and S_2 for the particle cloud height in Paper II. However, in the investigation of the continuous-phase instability (Paper I), only one dominant MI frequency ($S_{MI} = 0.06$), similar to Montes et al. [41] ($S_MI = 0.057$), could be observed.

The periodic phenomena were particle-size independent, the Strouhal number was identical for all particle sizes as was the amplitude. Increasing particle concentration did not affect the dominant frequencies (Strouhal numbers) in the spectra, but affected the distribution of the energy ratio. The amplitude of the higher frequency phenomena (S_2) decreased significantly, until the peak merged with the background signal. The lower frequency phenomena (S_1) not only stayed significant, but even increased its signal-to-noise ratio. Figure 5.12 shows the energy spectra of the 2mm particle suspension at two different concentrations.

With the particle density tracking method (Chap. 3.3.6) it was possible to

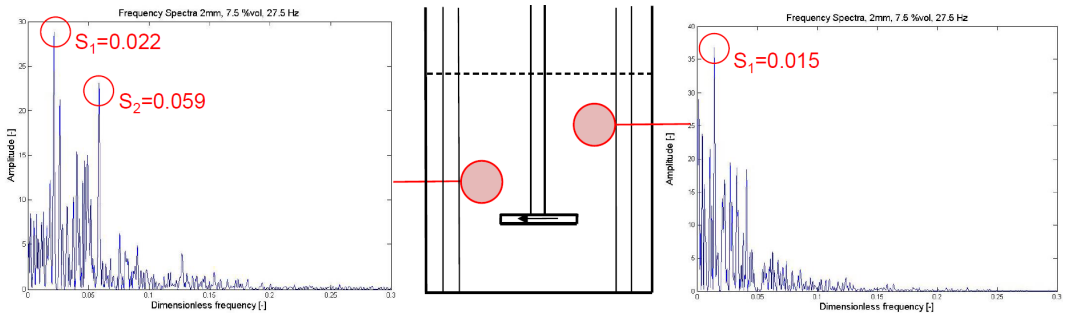

Figure 5.13: Cloud height spectra at different regions in the mixing vessel

identify periodic behaviours in different regions of the particle loud, however, it was not possible to look into the cloud itself, because the experimental setup was limited to a particle cloud near the wall. The particle density method delivered spectra, which are identical to the ones from the cloud height tracking, if evaluated at the same location and conditions. Evaluations at different locations in the vessel (fig. 5.13) showed that the amplitude of the two different Strouhal numbers (S_1 and S_2) varied. S_1 was the strongest in the upper third of the vessel and even present on the leeward side of the baffle, while S_2 decreased in amplitude when moving toward the leeward side of the baffle (right in all figures). S_2 was the strongest on the windward side of the baffles (left in all figures) and reached its maximum amplitude at approximately 1/3H, which corresponds to the impeller height.

For the particle cloud periodicities in Paper IV, it is suggested that the lower frequency (S_1) is connected to regular, but weaker, eruptions of particles from the cloud into the upper region of the vessel. The higher identified periodicity (S_2) is probably connected to the macro instability of the continuous phase. Figure 5.13 illustrates the amplitude of the different Strouhal numbers at different locations in the vessel, which shows additional similarities to the identified MI distribution of the continuous phase. Bittorf and Kresta [5] and Jahoda et al. [12] have concluded in their studies that the amplitude of the continuous

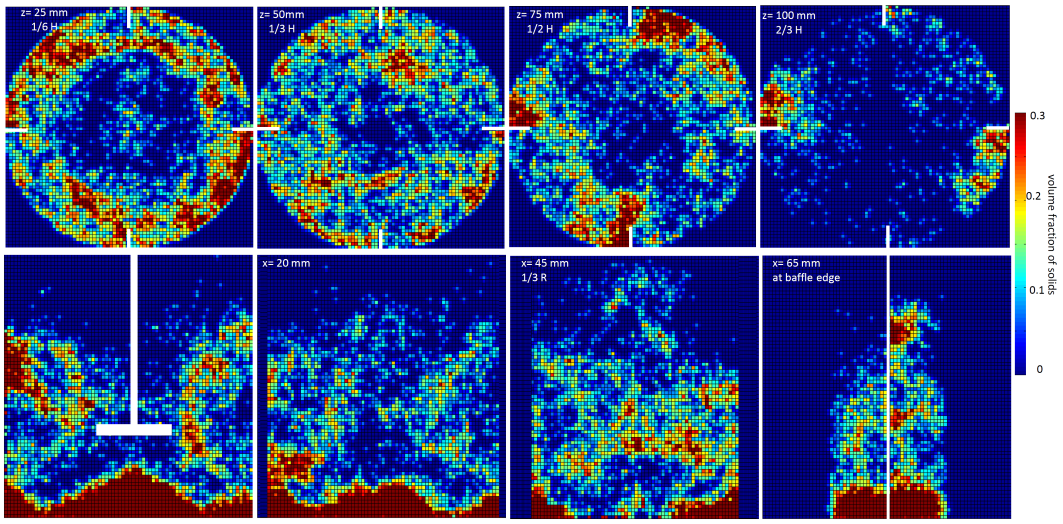

Figure 5.14: Local particle concentration at different vertical and horizontal planes(2mm 9.5%vol)

phase is dampened at higher solid concentrations, and that the MI disappears above the particle cloud. This is in agreement with the behaviour of the particle cloud periodicity S_2, the amplitude of which decreased with greater volume fraction. This behaviour could not be observed for S_1. Nevertheless, the experimental data (Paper I) show that the continuous phase MI is present at relatively high solid concentrations and above cloud height, but with lower amplitude.

With the CFD simulations and the evaluation algorithm it is possible to obtain detailed information from the inside of a particle cloud. The instantaneous local particle concentration has been analysed and visualized in Figure 5.14 for a 9.5%vol 2mm particle suspension. As described in the experimental observations, strong spatial variations of particle distribution could be identified. Particles were blocked on the windward side of the baffles and carried upwards by the baffle jets, eruptions of particles were mixed towards the centre of the vessel. High local particle concentrations could be found on the bottom of the vessel and at the edges of the vessel, but also in the upper regions of the vessel

in the vicinity of a wall.

With the cloud surface detection method (Chap. 4.2.2) it was possible to obtain a three-dimensional analysis of the particle cloud surface from the CFD simulations. Figure 4.4 shows a snapshot of the cloud surface in the 9.5%vol 2mm suspension at two different time steps. At one time step, the cloud height varied between 50mm (1/3H) and 120mm for different locations. This shows the strong spatial variation of cloud height, for which the baffle jets are the main contributors.

6

Conclusions and Outlook

This study has shown that it is possible to measure solid-liquid suspensions using the LDV system in very good temporal and spatial detail. The measurements have shown to be reliable and allow for comparisons between different conditions. With the LDV technique it was possible to determine velocity distributions, and consequently, energy spectra at high solid concentrations. Numerical models were developed to simulate flow structures in solid-liquid suspensions and results were compared to experimental data. Video processing methods were developed to investigate particle cloud formation in mixing vessels. The main focus was given to periodic phenomena in the flow field. Therefore, methods were developed to identify the spectra of a flow and to compare the frequency and amplitude between different flow conditions. The Lomb algorithm served well to analyse dominant frequencies in the flow. The amplitude-over-noise value showed little sensitivity to changes in the data rate and made it possible to determine and quantitatively evaluate the significance of the frequency of periodic phenomena at different flow conditions.

In the experimental study of the continuous phase in a mixing vessel (Paper I) it was possible to identify strong low frequency phenomena (MI), which dominated temporal variations of flow in the vessel. The dominant frequency was proven to be linear with impeller speed, resulting in a constant Strouhal number $S_{MI} = 0.059$. The frequencies of the MI phenomena were not affected by the addition of particles. However, the amplitude of the MI decreased with greater particle concentration. Different locations in the vessel experienced this decrease at different rates, but it was found at all locations in the vessel. Nevertheless, MI phenomena could still be identified under the maximal measurable solid concentration of 11.8%vol.

Studies focused on the particle phase showed that a particle cloud is characterized by strong local and temporal variations. When evaluating the spectra of temporal cloud height variations, two dominant frequencies were identified. The dominant frequencies were linear with impeller speed, and, therefore, described with a constant Strouhal number. The frequencies of the two phenomena ($S_1 = 0.02 - 0.03$ and $S_2 = 0.05 - 0.06$) were not influenced by the solid concentration or the size of particles. The amplitude of the periodicity showed no particle-size dependency, however, with higher particle concentration the amplitude of S_1 increased while the amplitude of S_2 showed a significant decrease. The two identified frequencies can be related to different phenomena in a particle cloud. The low frequency (S_1) is connected to eruptions on the cloud surface, and carries particles to the vessel top. The high frequency periodicity (S_2) was in the range of the continuous-phase macro instability, it was the strongest on the windward side of the baffle and decreased its amplitude with greater concentrations.

Numerical investigations of the macro instability of the continuous phase have proven to be in reasonable agreement with experimental findings. Periodic flow instabilities could be reproduced in the single-phase as well as in the solid-liquid suspension model. Using a Large Eddy Simulation (LES), the MI phenomena could be captured and reproduced with reasonable agreement ($S = 0.073$). The amplitude of the MI was lower at large volume fractions of solid particles. Simulations with larger particles delivered a significantly more pronounced MI amplitude than simulations with smaller particles.
With the discrete-phase simulations it was possible to evaluate the local particle concentration at any location in a vessel and identify the strong inhomogeneities and temporal variations. The surface of a particle cloud could be identified and tracked with the developed model. The spectral evaluation of the particle cloud dynamics was very time demanding, especially when considering the lower frequency region. Nevertheless, the obtained results show reasonable agreement with the experimental data. Two dominant frequencies were detected, the lower one agreed very well with the region of S_1. The second dominant periodicity was detected at slightly higher frequencies than S_2 in the experiments.

In the confined solid-liquid jet, two regions could be identified in which the flow was dominated by different phenomena vital to the transport of particles. The region in the vicinity of the nozzle featured high flow velocities and a well-defined shear layer with high turbulence. The flow was characterized by a small integral length scale and a large particle Stokes number in this region. With the addition of particles, an increase in RMS at the core of the jet and in the jet shear layer was observed. The increase was the most significant in the local minimum of the RMS profiles; the jet core. With an increase in particle size, an increase in the effect of particles on RMS values could be observed. The

axial velocity of the flow did not show any significant changes caused by the presence of particles.
The region farther away from the nozzle was dominated by large fluctuations; jet instabilities. Particles could follow these large-scale vortices well, as described by the low particle Stokes number in this region. In fact, it could be seen that jet instability was the main cause for the lateral distribution of solid particles into the fluid bulk. The large particles had a stabilizing effect on the jet and caused the instability to move farther downstream, while the frequency remained the same.

In future work it would be of interest to perform a deeper investigation of the mechanisms which drive the interaction between suspended and continuous phases. The formation of particle cloud height, flow structures of the continuous phase and periodic instabilities are important phenomena and require further research to understand the driving mechanisms of the formation of a particle cloud. Very little is known about the behaviour of non-uniform particle suspensions. How particles of different sizes organize and interact in a mixer would be of great interest for many processes, e.g. crystallization. In the field of numerical simulations, it is of great interest to progress further in discrete-phase modelling. Developments in collision modelling, the consideration of fluid displacement and the influence of local particle concentration would entail substantial progress for numerical simulations of solid-liquid suspensions.

List of Figures

List of Tables

Bibliography

[1] C. T. Crowe, M. Sommerfeld, Y. Tsuji, Multiphase flows with droplets and particles, CRC Press Inc, 1997.

[2] R. A. Gore, C. T. Crowe, International Journal of Multiphase Flow 15 (1989) 279–285.

[3] J.-i. Choi, O. Kwon, C. Lee, Journal of Physics: Conference Series 318 (2011) 052012.

[4] P. Hasal, J. Montes, H. Boisson, I. Fort, Chemical Engineering Science 55 (2000) 391–401.

[5] K. Bittorf, S. Kresta, Chemical Engineering Research and Design 81 (2003) 568–577.

[6] W. Bujalski, K. Takenaka, S. Paolini, M. Jahoda, A. Paglianti, K. Takahashi, A. Nienow, A. Etchells, Trans. IChemE (1999) 241 – 247.

[7] T. Zwietering, Chemical Engineering Science 9 (1958) 244–253.

[8] J. Kilander, F. Svensson, A. Rasmuson, AIChE journal 52 (2006) 4039–4051.

[9] M. Yianneskis, Z. Popiolek, J. Whitelaw, Journal of Fluid Mechanics 175 (1987) 537–555.

[10] D. Chapple, S. M. Kresta, Chemical engineering science 49 (1994) 3651–3660.

[11] C. Galletti, a. Paglianti, K. C. Lee, M. Yianneskis, AIChE Journal 50 (2004) 2050–2063.

[12] M. Jahoda, V. Machon, L. Vlach, I. Fort, Acta Polytechnica (2002) 3–7.

[13] A. Paglianti, G. Montante, F. Magelli, AIChE Journal 52 (2006) 426–437.

[14] M. Sardeshpande, V. Juvekar, V. Ranade, AIChE Journal 56 (2010) 2795–2804.

[15] O. Bruha, I. Fort, P. Smolka, Acta Polytechnica (1993).

[16] T. Bruha, P. Smolka, M. Jahoda, I. Fort, Chemical Engineering Research and Design 89 (2011) 2279–2290.

[17] A. A. Townsend, Journal of the Franklin Institute 262 (1956) 517.

[18] J. Hinze, Turbulence, Mcgraw-Hill College, 1975.

[19] I. Wygnanski, H. Fiedler, Journal of Fluid Mechanics 38 (1969) 577–612.

[20] G. Batchelor, A. Gill, Journal of Fluid Mechanics 14 (1962) 529–551.

[21] J. Fan, H. Zhao, K. Cen, Experiments in Fluids 287 (1992) 279–287.

[22] H. Sheen, B. Jou, Y. Lee, Experimental Thermal and Fluid Science (1994) 315–327.

[23] Y. Hardalupas, A. Taylor, J. Whitelaw, Proceedings of the Royal Society of London. A. Mathematical and Physical Sciences 426 (1989) 31–78.

[24] R. N. Parthasarathy, in: ASME/JSME Fluids Engineering and Laser Anemometry Conference and Exhibition, volume 228, pp. 427 – 433.

[25] T. Virdung, a. Rasmuson, Chemical Engineering Science 62 (2007) 5963–5978.

[26] F. Durst, A. Melling, J. H. Whitelaw, Principles and Practice of Laser-Doppler Anemometry, Academic Press, 1981.

[27] N. R. Lomb 39 (1976).

[28] W. H. Press, S. A. Teukolsky, W. T. Vetterling, B. P. Flannery, Numerical Recipes in C, volume 29, Cambridge University Press, 1992.

[29] G. I. Taylor, Proceedings of the Royal Society of London Series A Mathematical and Physical Sciences 164 (1938) 476–490.

[30] Pope, Turbulent flow, Cambridge University Press, 2000.

[31] D. Lilly, IBM Scientific Computing Symposium on Environmental Sciences (1967) 195.

[32] J. Smagorinsky, Mon. Weather Rev. 91 (1963) 99–164.

[33] D. K. Lilly, Physics of Fluids A: Fluid Dynamics 4 (1992) 633.

[34] S. a. Morsi, a. J. Alexander, Journal of Fluid Mechanics 55 (1972) 193.

[35] S. Apte, K. Mahesh, T. Lundgren, International Journal of Multiphase Flow 34 (2008) 260–271.

[36] S. B. Pope, New Journal of Physics 6 (2004) 35–35.

[37] S. Benayad, A. Salem, J. Legrand, Journal of Applied electrochemistry 30 (2000) 209–216.

[38] K. J. Bittorf, S. M. Kresta, AIChE Journal 47 (2001) 1277–1284.

[39] M. Jahoda, M. Mostek, I. Fort, P. Hasal, The Canadian Journal of Chemical Engineering 89 (2011) 717–724.

[40] V. T. Roussinova, S. M. Kresta, R. Weetman, AIChE Journal 50 (2004) 2986–3005.

[41] J. Montes, H. Boisson, I. Fort, Chemical Engineering Journal 67 (1997) 139–145.